

Multi-Species Cohesion: Humans, machinery, AI and beyond

Frank Yingjie Huo, Pedro D. Manrique, and Neil F. Johnson

Physics Department, George Washington University, Washington, DC 20052, U.S.A.

(Dated: February 1, 2024)

What large-scale cohesive behaviors – desirable or dangerous – can suddenly emerge from systems with interacting humans, machinery and software including AI? When will they emerge? How will they evolve and be controlled? Here we offer some answers to these urgent questions by introducing an aggregation model that accounts for entities’ inter- and intra-species diversities. It yields a novel multi-dimensional generalization of existing aggregation physics. We derive exact analytic solutions for the time-to-cohesion and growth-of-cohesion for two species, and some generalizations for an arbitrary number of species. These solutions reproduce – and offer a microscopic explanation for – an anomalous nonlinear growth feature observed in related real-world systems, e.g. Hamas-Hezbollah online support, human-machine team interactions, AI-determined topic coherence. A key takeaway is that good and bad ‘surprises’ will appear increasingly quickly as humans-machinery-AI etc. mix more – but the theory offers a rigorous approach for understanding and controlling this.

Each of us will soon become – or are already – part of some large-scale, decentralized system comprising different types of interacting humans, different types of technological machinery including sensors and actuators, and/or different types of AI and other smart software [1–4]. In addition to AI-enabled human-bot social media systems post-GPT, and the looming Metaverse, there is a race toward AI-assisted, large-scale human-machine systems in everything from commerce, medicine and defense through to space exploration [1–4]. For situations involving machine-learning and AI, the interacting entities will include different categories of informational data tokens or topics extracted from some unstructured multimodal dataset of text, images, audio, video etc. [5–13]. In all cases, these diverse entities’ interactions will be largely remote, online or in some more abstract space. Physical separations are essentially irrelevant.

This raises key questions for both Society and fundamental science around what large-scale cohesive behaviors may suddenly appear from out-of-nowhere in such mixed systems? When? How will they evolve and be controlled? And what novel insights can Physics add to address these questions? The spontaneous, bottom-up emergence of system-level cohesion may be desirable (e.g. emergence of cooperation and coordination in a human-AI-robot surgical team or space mission). But it may be undesirable and even highly dangerous, particularly if such systems belong to adversaries (e.g. emergence of AI-assisted online extremism) [14, 15]. Our use of the term ‘cohesion’ here is consistent with the huge body of existing physics on polymers, networks etc. [16–27], i.e. we take it to mean the sudden, spontaneous emergence and growth of some macroscopic unit (‘cohesive unit’) containing a non-negligible fraction of the entire multi-species population. In more traditional physics settings with identical entities, this ‘cohesive unit’ represents the well-known gel, or giant connected component (GCC), or it could be a cartoon of some dynamically emerging coherent many-body state [19–26, 28].

Here we offer some answers to these questions by introducing a simple physics model that permits some exact

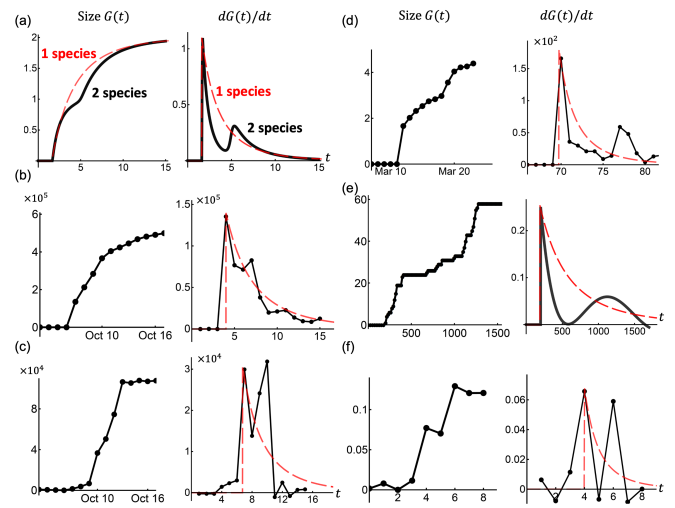


FIG. 1. Sudden emergence and growth of a cohesive unit ($G(t)$ and its derivative) in several existing real-world systems that mix humans, machinery and/or AI. (a) Our theory’s predicted growth features for $D = 2$ species. Additional kinks appear for $D > 2$. (b), (c): Emergence of Hamas and Hezbollah online support from interacting humans, bots, social media machinery, surrounding 2023 Israel attack [29]. (d) Emergence of anti-U.S. jihadi online support from interacting humans, bots, social media. (e) Emergence of team-level activity in mixed human-machinery-software system during aerospace missions [1]. Derivative is calculated for a smoothed $G(t)$. (f) Emergence of topic coherence (a well-known AI measure capturing ‘meaning’ [5, 6]) in machine learning-AI analysis of tokens’ embeddings from human-machine multimodal data [5, 6]. Ref. [7] shows strikingly similar growth curves also arise for the sudden emergence of AI abilities.

analytic solutions, and that reproduces the sudden appearance and anomalous growth feature observed in several related real-world systems (see Fig. 1), each of which will probably feature in future human-machinery-AI super-systems. The novelty of the new theory and model lies in allowing different species of entity and diversity within each species, and for any number of species D . We use

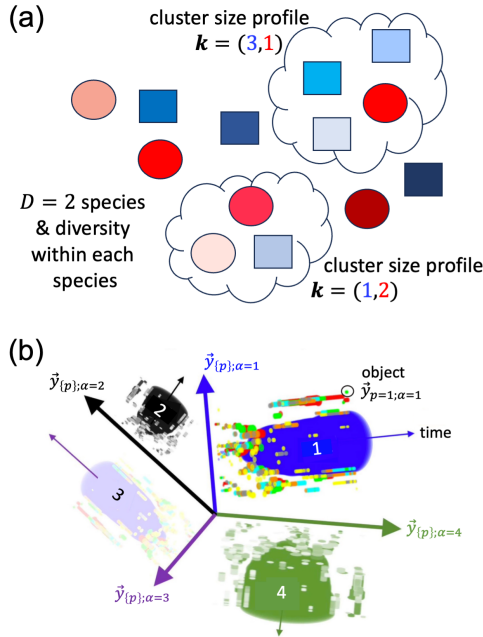


FIG. 2. (a) Schematic of our theory at a given timestep for $N = 13$ interacting entities drawn from across $D = 2$ species (i.e. circles and squares). The spectra of colors for an entity of each species represents its intra-species traits. (b) Our theory’s output in the absence of cross-species aggregation (i.e. off-diagonal F elements all zero). Adding cross-species aggregation (some or all F elements non-zero) leads to the sudden emergence of anywhere between 1 and D cohesive units along different (mixed) directions, each with their own onset time and each with its own mixed-species composition.

the classification term ‘species’ to represent some major difference between entities that is relevant to the overall system dynamics. Remaining differences between entities are represented as intra-species heterogeneity. Different species could be different types of humans, machinery, AI, or any mix of these. Hence our study expands formal physics understanding by showing how existing dynamical equations for interacting identical particles/nodes [30–35] generalize to new application domains (e.g., human-machinery-AI) involving $D > 1$ species of objects and within-species diversity.

Figure 1 shows that even the simple two-species limit of this new theory, captures the anomalous kink-like growth feature observed in the example systems – and offers a microscopic interpretation. To explain this, we first lay out the theory, deferring step-by-step mathematical derivations to the Supplementary Material (SM). Numerical simulations show that our exact and approximate analytical results in this paper are accurate (see SM).

We start with a general system containing $N = \sum_{\alpha=1}^D N_{\alpha}$ indivisible entities of D major types (species) where the species label α denotes a dominant characteristic of each entity that does not change significantly over time. Different species could represent different types of humans or machines, or the same type of ma-

chines (software/AI) from different manufacturers (developers); or different categories of tokens or topics within AI/ Large Language Models like GPT, DALL-E. Each entity p within a given species α can have an arbitrary number of additional intra-species traits which could in principle change over time, denoted as $\vec{y}_{p,\alpha}(t)$ where each component (trait value) lies between 0 and 1 following Refs. [22, 36–43].

Similar to embedding in machine learning and AI, each entity is hence a vector in some high dimensional space. Certain dimensions denote major characteristic differences (i.e. species label α) while others represent the diversity within each species (Fig. 2). As a result of interactions, some entities may find themselves at any time either coordinated, correlated or just interrelated in some way, hence forming effective clusters that can change in size, composition and total number over time (Fig. 2(a)). The *cluster size profile* for each cluster at a given timestep is $\mathbf{k} = (k_1, k_2, \dots, k_D)$ where k_{α} is the number of species- α entities. Each cluster’s total size is $k = \sum_{\alpha=1}^D k_{\alpha}$. The number of clusters with the same size profile \mathbf{k} is $n_{\mathbf{k}}$. Since $N_{\alpha} \gg 1$, we take $N_{\alpha} = N/D$ for simplicity. If all cross-species interactions are zero, we would see up to D separate cohesive units (and hence up to D good or bad ‘surprises’) emerge spontaneously over time, each of which contains just a single species of entity (Fig. 2(b)).

References [36, 44–46] showed that the aggregation mechanism in various human/machine(bots)/online-communications systems has an approximate product kernel form which we therefore adopt, though this can be easily generalized (see SM Sec. VII B). Specifically, two randomly chosen entities fuse together at each timestep – and if they are already part of a cluster, their entire clusters fuse together. We add here the additional feature that the fusion probability is some general function of the pair’s similarity $S_{\alpha\beta}(\vec{y}_{1;\alpha}, \vec{y}_{2;\beta}, t)$ (e.g., $|\vec{y}_{1;\alpha}(t) - \vec{y}_{2;\beta}(t)|$) since cross-species and intra-species aggregation will generally occur at different rates. A D -dimensional fusion probability matrix F can be calculated by averaging the pair similarity function $S_{\alpha\beta}(\vec{y}_{1;\alpha}, \vec{y}_{2;\beta}, t)$ over the population distribution (see SM). Even if some $\vec{y}_{p;\alpha}$ terms vary quickly in time, the population average quantities in F will likely not. For non-binary fusion (i.e., multi-body fusion from coordinated aggregation such as influence campaigns), F will be a higher-order tensor.

The general form for the cluster fusion dynamics within this mixed-entity (e.g., humans, machinery, AI) system then becomes (see SM for detailed derivation):

$$\frac{d\nu_{\mathbf{k}}}{d\tau} = \frac{1}{2D} \sum_{\mathbf{k}=i+j} \mathbf{i}^T F \mathbf{j} \nu_i \nu_j - \mathbf{k}^T F \left(\frac{N}{N} \right) \nu_{\mathbf{k}} + g(\mathbf{k}, \tau) \quad (1)$$

where the dimensionless quantity $\nu_{\mathbf{k}} = (D/N)n_{\mathbf{k}}$ and $\tau = 2t/N$ is a rescaled time. A function $g(\mathbf{k}, \tau)$ appears if higher-order interactions are included, e.g. ≥ 3 -body aggregation processes such as in coordinated influence campaigns (SM Sec. VII). As well as generalizing the

Smoluchowski equation [32], Eq. (1) is exactly equivalent to a D -dimensional generalization of the inviscid Burgers' equation plus additional shear interactions (see SM using $\varepsilon_\alpha(\mathbf{x}, \tau) = \sum_{\mathbf{k}} k_\alpha \nu_{\mathbf{k}} e^{-\mathbf{k} \cdot \mathbf{x}}$):

$$\frac{\partial \varepsilon_\alpha}{\partial \tau} + \frac{1}{D} F_{\beta\gamma} (\varepsilon_\beta - \nu_\beta) \partial_\gamma \varepsilon_\alpha - \partial_\alpha \tilde{g}(\mathbf{x}, \tau) = 0 \quad . \quad (2)$$

The constant vector $\nu_\beta = 1 \forall \beta = 1, \dots, D$. $\tilde{g}(\mathbf{x}, \tau)$ is the Laplace transformation of $g(\mathbf{k}, \tau)$.

The solution to Eq. (2) at $\mathbf{x} = 0$ gives the time-dependent growth of the mixed-species cohesive unit(s) that will emerge: $G(\tau) = 1 - \sum_{\alpha=1}^D \varepsilon_\alpha(\mathbf{0}, \tau)/D$ (i.e. $G(t)$ in Fig. 1). For binary fusion (i.e. $g(\mathbf{k}, \tau) = 0$) and all-monomer initial condition, Eq. (2) can be solved analytically (see SM):

$$G(\tau) = 1 - \frac{1}{D} \sum_{\alpha=1}^D e^{-\sum_{\beta} F_{\alpha\beta} G_\beta(\tau) \tau / D}, \quad (3)$$

where $G_\beta(\tau) \equiv 1 - \varepsilon_\beta(0, \tau)$ is the proportion of species- β entities in the cohesive unit. A given cohesive unit μ 's onset time (i.e. time-to-cohesion) is given by the eigenvalue λ_μ of F where $\mu = 1, \dots, D$, i.e., $(\tau_g)_\mu = D/\lambda_\mu$. Its composition is given by the corresponding eigenvector $\mathbf{x}^{(\mu)}$, i.e. $\mathbf{k}^{(\mu)}$ such that $\mathbf{k}^{(\mu)} \cdot \mathbf{x}^{(\nu)} = \delta_{\mu\nu}$. $\mathbf{k}^{(\mu)}$ represents a real-world cohesive unit only if all its components are non-negative. Up to D such mixed-species cohesive units *could* emerge – but any cohesive unit with an infinite or negative onset time will never appear.

This has a key real-world implication: we can predict the number of future cohesive units that will emerge – and hence good or bad ‘surprises’ as in Fig. 1 – and their onset times, simply by analyzing the properties of F . (Their growth can then be calculated using Eq. (3) or more generally Eq. (2).) Specifically, we organize F into block-diagonal form: each submatrix F_s ($s = 1, \dots, d$ where d is the number of submatrices) then represents a separate and generally mixed-species cohesive unit. In the absence of cross-species aggregation (i.e. diagonal F) $d = D$ and each cohesive unit comprises a single species (Fig. 2(b)). For cases where each F_s is symmetric and non-negative, the Perron-Frobenius theorem ensures that it has only one non-negative eigenvector, labelled as $\mathbf{x}_{\max}^{(s)}$, corresponding to the largest eigenvector $\lambda_{\max}^{(s)}$. Hence for each irreducible subsystem F_s , there exists exactly one onset of a cohesive unit at $\tau_g^{(s)} = D/\lambda_{\max}^{(s)}$, with composition given by the $\mathbf{k}_{\max}^{(s)}$. Each can be found exactly. This can be understood by imagining gradually turning on all the cross-species aggregation entries starting from a diagonal F (i.e., off-diagonal entries become non-zero): hence F finally becomes irreducible which mathematically has the effect of rotating the principal axes of F until all but one of the eigenvectors have at least one negative component – hence only one mixed-species cohesive unit would emerge. In general, the total number of emerging cohesive units (future ‘surprises’) will lie between 1 and D .

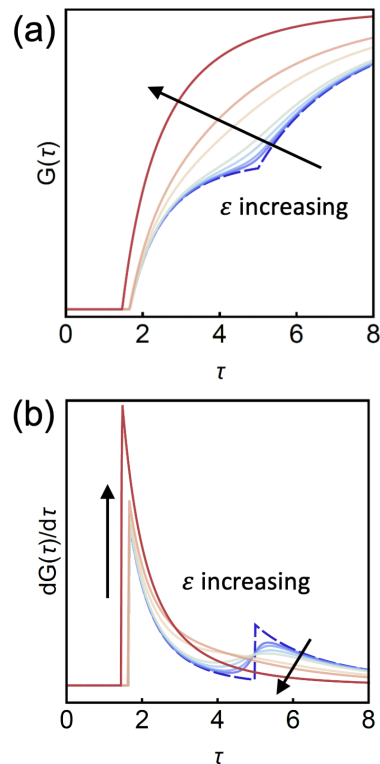


FIG. 3. (a) Our theory’s predicted cohesive unit size $G(\tau)$ versus (scaled) time τ for $D = 2$ species system ($G(\tau) = (1/2) \sum_{\alpha=1}^2 G_\alpha(\tau)$). Shown for increasing values of the cross-species aggregation terms with off-diagonal terms in 2×2 matrix F all set to ϵ for simplicity. (b) $dG(\tau)/d\tau$. For $\epsilon = 0$, dashed lines show two discontinuities corresponding to two separate cohesive unit onsets. But as ϵ increases, the physically observed onset moves to earlier times, while the latter becomes virtual. The ‘ghost’ cohesive-unit kink can be thought of as an alternative what-if future of the system, assuming the earlier portion were somehow quashed or removed.

An exact analytical solution can be derived (see SM) for any number of species D , in the case that all intra-species terms are identical (i.e. all diagonal entries in F equal to f) and all inter-species terms are identical (i.e. all off-diagonal entries equal to ϵ). The Perron-Frobenius theorem ensures that $\mathbf{k}^{(0)} = (1, \dots, 1)/\sqrt{D}$ is the only cohesive unit that will emerge, with an exact onset time

$$\tau_g = D[f + (D - 1)\epsilon]^{-1} \quad . \quad (4)$$

Key practical implications of Eq. (4) are: (i) cohesive units (and hence good and bad ‘surprises’) will appear sooner as humans-machinery-AI etc. mix more (i.e. τ_g decreases as ϵ and/or f increase); (ii) as the number of species increases ($D \rightarrow \infty$), $\tau_g \rightarrow \epsilon^{-1}$, hence the system eventually behaves like a renormalized one-species system in which the intra-species aggregation probability is now ϵ instead of f . f becomes irrelevant. Eq. (4) is also a good approximation when the relevant F entries are similar but not identical.

Focusing now on the analytically simplest case of $D =$

2 species, Figs. 3(a)(b) show that the model's exact solution from Eq. (3) predicts a kink structure in the total cohesive unit growth (G and $dG/d\tau$) as in Fig. 1. As ϵ increases from 0, the kink ('ghost' cohesive unit) gets smeared out. Higher D will generate more kinks – but this $D = 2$ result already mimics Fig. 1's real-world growth behavior. It hence offers a plausible microscopic interpretation for all the diverse examples in Fig. 1: a subset of entities from across species get involved immediately while the others act collectively *as if* they are sitting on-the-fence, even though there is no such individual-level mechanism in the model. We hope this motivates deeper social science analysis beyond this paper's necessarily limited scope.

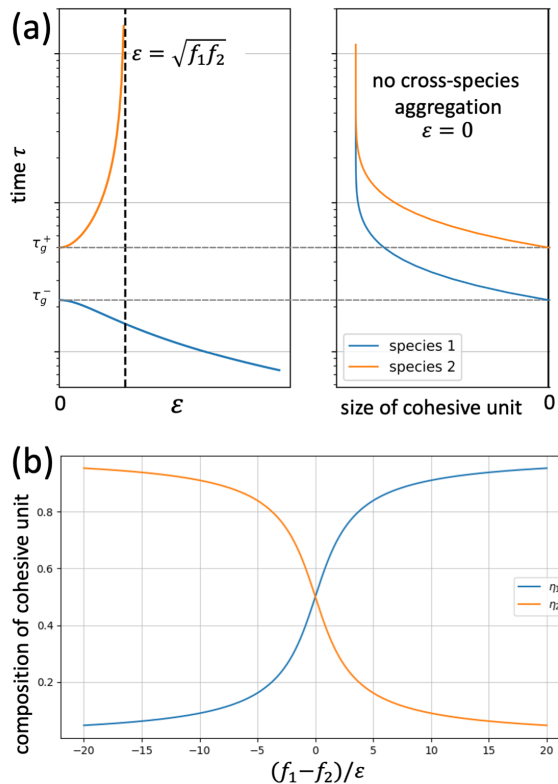


FIG. 4. (a) Left: cohesive unit onset time (i.e. time-to-cohesion) as a function of inter-species interaction ϵ . When $\epsilon = 0$, both onsets occur separately; but as ϵ increases, the cohesive unit will appear earlier, while the ‘ghost’ appears later and eventually disappears. This means that increasing the cross-species aggregation in future mixed systems will make good and bad ‘surprises’ appear earlier. Right plot depicts the separate contributions to $G(\tau)$ at $\epsilon = 0$. (b) Proportions of the two species in the cohesive unit as a function of $\sigma \equiv (f_1 - f_2)/\epsilon$: larger σ values denote increasing relative asymmetry in the intra-species aggregation probabilities and hence higher asymmetry in the cohesive unit’s composition.

To understand more deeply the general nature of this kink in the growth (Figs. 1(a) and 3), we consider $D = 2$

with *non*-identical diagonal F elements f_1, f_2 . The 2×2 F matrix has two roots:

$$\tau_g^{(1,2)} = [(f_1 + f_2) \mp \sqrt{(f_1 - f_2)^2 + 4\epsilon^2}] [f_1 f_2 - \epsilon^2]^{-1} . \quad (5)$$

Fig. 4(a) shows that the variation of these two roots with ϵ is strikingly similar to the hybridization in a 2-band model from solid state physics [47]. When $\epsilon = 0$, the two species form separate single-species cohesive units at times $\tau_g^{(1,2)} = 2/f_{1,2}$. Turning on the cross-species interaction (i.e. $\epsilon > 0$) there is a transition such that only one mixed-species cohesive unit emerges at $\tau_g^{(1)}$. As ϵ grows larger, $\tau_g^{(1)}$ becomes smaller hence the mixed-species cohesive unit forms earlier in agreement with Fig. 3(a). By contrast, the larger root $\tau_g^{(2)}$ increases: but instead of a real onset, it denotes a ‘virtual’ one driven by the latency of the slower-aggregating species – hence the kink. $\tau_g^{(2)}$ then diverges at $\epsilon^2 = f_1 f_2$, and for $\epsilon^2 > f_1 f_2$ there is only one positive root and the kink disappears. An analytic solution for the cohesive unit’s composition just after onset, comes from either Taylor expanding Eq. (3) or calculating $\mathbf{k}^{(1,2)}$ (see SM Sec. IV). The composition of species α in this cohesive unit η_α , depends solely on $\sigma \equiv (f_1 - f_2)/\epsilon$ (plotted in Fig. 4(b)):

$$\eta_1 = 2 \left[\sqrt{\sigma^2 + 4} - \sigma + 2 \right]^{-1} \quad (6)$$

$$\eta_2 = 1 - \eta_1 = 2 \left[\sqrt{\sigma^2 + 4} + \sigma + 2 \right]^{-1} . \quad (7)$$

The cohesive unit’s composition is hence highly sensitive to small asymmetries in the two intra-species aggregations (i.e. σ). This has a key real-world implication: too much symmetry in different species’ internal aggregation probabilities will make the cohesive unit’s composition unstable, and hence taking for granted that system behaviors have a particular composition is risky.

Beyond the Physics, this work offers a takeaway for Society: good and bad ‘surprises’ (i.e., sudden emergence of cohesive units) will appear increasingly quickly as humans-machinery-AI etc. mix more – but a Physics approach such as this can offer a rigorous understanding and test-bed for control interventions. Our multi-species theory is obviously simplistic. However, this makes it generic enough to apply at many scales and with many types of entities. We speculate that its focus on entities’ (tokens’) assembly could also help it provide a first microscopic explanation for how output and ability seem to suddenly ‘emerge’ [7] in machine learning, AI and even new Transformer architectures – with the caveat that encoding of the sequences of cluster assembly must then be taken into account via complex temporal terms in F .

This research is supported by U.S. Air Force Office of Scientific Research awards FA9550-20-1-0382 and FA9550-20-1-0383 and The Templeton Foundation.

- [1] J. C. Gorman, M. Demir, N. J. Cooke, and D. A. Grimm, Evaluating sociotechnical dynamics in a simulated remotely-piloted aircraft system: a layered dynamics approach, *Ergonomics* **62**, 629 (2019).
- [2] L. Huang, N. J. Cooke, R. S. Gutzwiller, S. Berman, E. K. Chiou, M. Demir, and W. Zhang, Chapter 13 - distributed dynamic team trust in human, artificial intelligence, and robot teaming, in *Trust in Human-Robot Interaction*, edited by C. S. Nam and J. B. Lyons (Academic Press, 2021) pp. 301–319.
- [3] Science and technology strategy, United States Air Force (2019), <https://www.af.mil/Portals/1/documents/2019SAFstoryattachments/AirForceScienceandTechnologyStrategy.pdf>.
- [4] Advancing artificial intelligence research infrastructure through new NSF investments, National Science Foundation (2023), <https://new.nsf.gov/news/advancing-artificial-intelligence-research>.
- [5] R. Sear, N. J. Restrepo, and N. F. Johnson, Dynamic topic modeling reveals variations in online hate narratives, in *Intell. Comp.*, edited by K. Arai (Springer International Publishing, Cham, 2022) pp. 564–578.
- [6] R. Sear, R. Leahy, N. J. Restrepo, and N. Johnson, Machine learning reveals adaptive Covid-19 narratives in online anti-vaccination network, in *Proc. of 2021 Conf. of Comp. Social Science Soc. of Americas*, edited by Z. Yang and E. von Briesen (Springer International Publishing, Cham, 2022) pp. 164–175.
- [7] J. Wei, Y. Tay, R. Bommasani, C. Raffel, B. Zoph, S. Borgeaud, D. Yogatama, M. Bosma, D. Zhou, D. Metzler, E. H. Chi, T. Hashimoto, O. Vinyals, P. Liang, J. Dean, and W. Fedus, Emergent abilities of large language models (2022), arXiv:2206.07682 [cs.CL].
- [8] A. Acharya, S. Sikdar, S. Das, and H. Rangwala, Gensyn: A multi-stage framework for generating synthetic microdata using macro data sources, in *IEEE International Conference on Big Data* (2022) pp. 685–692.
- [9] Y. Bromberg, P. Ramakrishnan, A. Kabir, and A. Shehu, Variant prediction in the age of machine learning (2023).
- [10] W. Fulkerson, R. Axtell, A. Deshmukh, V. Parunak, and W. Farrell, Unifying Themes In Complex Systems 2, 209 (2018).
- [11] J. P. Singh, Diffusion of power and diplomacy: New meanings, problem solving, and deadlocks in multilateral negotiations, *International Negotiation* **20**, 73 (2015).
- [12] J. J. Van Bavel, C. E. Robertson, K. del Rosario, J. Rasmussen, and S. Rathje, Social media and morality, *Annual Review of Psychology* **75**, 311 (2024), PMID: 37906950, <https://doi.org/10.1146/annurev-psych-022123-110258>.
- [13] D. Rogers, Can AI get rid of fake news and other misinformation?, Gobaal Summit: AI for Good 2024 (2022), <https://aiforgood.itu.int/speaker/daniel-rogers/>.
- [14] J. M. Berger and H. Perez, The Islamic State’s diminishing returns on Twitter, GW program on extremism (2016), <https://extremism.gwu.edu/sites/g/files/zaxdzs5746/files/downloads/JMBDiminishingReturns.pdf>.
- [15] C. Miller-Idriss, *Hate in the Homeland* (Princeton University Press, 2022).
- [16] W. H. Stockmayer, Theory of molecular size distribution and gel formation in branched-chain polymers, *J. Chem. Phys.* **11**, 45 (1943).
- [17] W. H. Stockmayer, Theory of molecular size distribution and gel formation in branched polymers II. general cross linking, *J. Chem. Phys.* **12**, 125 (1944).
- [18] P. J. Flory, *Principles of polymer chemistry* (Cornell University Press, 1953).
- [19] P. L. Krapivsky, S. Redner, and E. Ben-Naim, *A Kinetic View of Statistical Physics* (Cambridge University Press, 2010).
- [20] A.-L. Barabási, *Network Science* (Cambridge University Press, 2016).
- [21] M. Newman, *Networks* (Oxford University Press, 2018).
- [22] A. Soulier and T. Halpin-Healy, The dynamics of multidimensional secession: Fixed points and ideological condensation, *Phys. Rev. Lett.* **90**, 258103 (2003).
- [23] F. Schweitzer and G. Andres, Social nucleation: Group formation as a phase transition, *Phys. Rev. E* **105**, 044301 (2022).
- [24] X. Niu, C. Doyle, G. Korniss, and B. Szymanski, The impact of variable commitment in the naming game on consensus formation, *Sci Rep* **7**, 41750 (2017).
- [25] P. S. Dodds, K. D. Harris, I. M. Kloumann, C. A. Bliss, and C. M. Danforth, Temporal patterns of happiness and information in a global social network: Hedonometrics and Twitter, *PLOS ONE* **6**, 1 (2011).
- [26] B. T. Fagan, N. J. MacKay, and A. J. Wood, Robustness of steady state and stochastic cyclicity in generalized coalescence-fragmentation models (2023), arXiv:2310.04226 [cond-mat.other].
- [27] M. Jusup, P. Holme, K. Kanazawa, M. Takayasu, I. Romić, Z. Wang, S. Geček, T. Lipić, B. Podobnik, L. Wang, W. Luo, T. Klanjšček, J. Fan, S. Boccaletti, and M. Perc, Social physics, *Physics Reports* **948**, 1–148 (2022).
- [28] X. Liu, J. I. A. Li, K. Watanabe, T. Taniguchi, J. Hone, B. I. Halperin, P. Kim, and C. R. Dean, Crossover between strongly coupled and weakly coupled exciton superfluids, *Science* **375**, 205 (2022), <https://www.science.org/doi/pdf/10.1126/science.abg1110>.
- [29] Data from Hamas’ and Hezbollah’s official communities on Telegram: <https://ir.tgstat.com/channel/@qassambrigades/stat>, <https://ir.tgstat.com/channel/@Hezbollah/stat>.
- [30] R. M. Ziff, E. M. Hendriks, and M. H. Ernst, Critical properties for gelation: A kinetic approach, *Phys. Rev. Lett.* **49**, 593 (1982).
- [31] E. M. Hendriks, M. H. Ernst, and R. M. Ziff, Coagulation equations with gelation, *J. Stat. Phys.* **31**, 519 (1983).
- [32] J. A. Wattis, An introduction to mathematical models of coagulation-fragmentation processes: A discrete deterministic mean-field approach, *Physica D: Nonlinear Phenomena* **222**, 1 (2006).
- [33] R. L. Drake, *A General Mathematics Survey of the Coagulation Equation* (Pergamon Press, 1972).
- [34] A. Lushnikov, Gelation in coagulating systems, *Physica D: Nonlin. Phen.* **222**, 37 (2006).
- [35] A. C. Nelson, J. P. Keener, and A. L. Fogelson, Kinetic model of two-monomer polymerization, *Phys. Rev. E* **101**, 022501 (2020).

- [36] P. D. Manrique, F. Y. Huo, S. El Oud, M. Zheng, L. Illari, and N. F. Johnson, Shockwavelike behavior across social media, *Phys. Rev. Lett.* **130**, 237401 (2023).
- [37] P. Lozano, S. Gavrillets, and A. Sanchez, Cooperation, social norm internalization, and hierarchical societies, *J. Stat. Phys.* **151**, 395–413 (2013).
- [38] P. Tornberg, How digital media drive affective polarization through partisan sorting, *PNAS* **119**, e2207159119 (2022).
- [39] D. Centola, J. Gonzalez-Avella, V. Eguiluz, and M. San Miguel, Homophily, cultural drift, and the co-evolution of cultural groups, *J. Confl. Resol.* **51**, 905 (2007).
- [40] N. F. Johnson, P. Manrique, and P. M. Hui, Modeling insurgent dynamics including heterogeneity, *J. Stat. Phys.* **151**, 395–413 (2013).
- [41] P. D. Manrique, P. M. Hui, and N. F. Johnson, Internal character dictates transition dynamics between isolation and cohesive grouping, *Phys. Rev. E* **92**, 062803 (2015).
- [42] P. D. Manrique and N. F. Johnson, Individual heterogeneity generating explosive system network dynamics, *Phys. Rev. E* **97**, 032311 (2018).
- [43] P. D. Manrique, M. Zheng, Z. Cao, E. M. Restrepo, and N. F. Johnson, Generalized gelation theory describes onset of online extremist support, *Phys. Rev. Lett.* **121**, 048301 (2018).
- [44] G. Palla, A.-L. Barabási, and T. Vicsek, Quantifying social group evolution, *Nature* **446**, 664 (2007).
- [45] P. Erdős and A. Rényi, On random graphs I, *Publicationes Mathematicae Debrecen* **6**, 290 (1959).
- [46] P. Erdős and A. Rényi, On the evolution of random graphs, *Publ. Math. Inst. Hungary. Acad. Sci.* **5**, 17 (1960).
- [47] N. F. Johnson, H. Ehrenreich, K. C. Hass, and T. C. McGill, f-sum rule and effective masses in superlattices, *Phys. Rev. Lett.* **59**, 2352 (1987).
- [48] F. Battiston, E. Amico, A. Barrat, G. Bianconi, G. F. de Arruda, B. Franceschiello, I. Iacopini, S. Kéfi, V. Latora, Y. Moreno, M. M. Murray, T. P. Peixoto, F. Vaccarino, and G. Petri, The physics of higher-order interactions in complex systems, *Nat. Phys.* **17**, 1093 (2021).

Supplementary Material

I. INTRODUCTION

The multi-species aggregation model that we present in this paper is a direct but highly nontrivial extension of the one that we previously reported [36]. This Supplementary Material (SM) constructs a systematic multi-species theory from generalizing the results in [36] as well as first principles, and the key results have been presented in the main paper. This SM is organized into the following Sections: in Section II we construct the formalism of the theory. This is followed by a detailed discussion for the general D -species model in Section III, and Sections IV and V derive key analytic results for $D = 2$ and 3 respectively. Section VI then discusses a specific class of the multi-species model which illustrates its convergence to the mean-field theory [36] at very large D values, and lastly in Section VII we further outline potential extensions of this theory.

II. MULTI-DIMENSIONAL AGGREGATION MODEL

Our D -dimensional aggregation model assumes that there are D different species of particles in the system, each undergoing aggregation both within its own species (just like the 1-dimensional model in [36]) and with different species. Moreover, the rates of aggregation are potentially different for these different combinations, as they could obey different mechanisms, and hence different mean-field parameters for aggregation rates. We begin with defining key quantities of the theory. As in the main paper, we denote the total number of particles in the system as N , and the number of particles in a particular species α ($\alpha = 1, 2, \dots, D$) is N_α . Together they can be written into a vector $\mathbf{N} = (N_1, N_2, \dots, N_D)$. By definition $N = \sum_{\alpha=1}^D N_\alpha$. Since $N_\alpha \gg 1$, we take $N_\alpha = N/D$ for simplicity in the upcoming analytics. To denote the constituents of a cluster compactly, we employ a vectorial notation of cluster size $\mathbf{k} = (k_1, k_2, \dots, k_D)$, where k_α is the number of particles of species α in this cluster. \mathbf{k} then represents the size profile of a specific cluster. It can be seen straightforwardly that cluster \mathbf{k} is a mixed cluster if two or more components of \mathbf{k} are non-zero. As before, functions $\{n_{\mathbf{k}}\}$ are the size distribution of clusters of profile \mathbf{k} , i.e. the number of clusters with a composition \mathbf{k} . So

$$N = \sum_{\mathbf{i}} i n_{\mathbf{i}}, \quad (8)$$

where $\sum_{\mathbf{i}}$ is shorthand for $\sum_{i_1=0}^{\infty} \sum_{i_2=0}^{\infty} \dots \sum_{i_D=0}^{\infty}$.

A. Master equations and the heterogeneity matrix

We begin by looking at what aggregation terms look like under multi-species aggregation. For single species, binary aggregation is realized by a simple scalar addition of sizes

$$k = i + j. \quad (9)$$

As a reference we first write down the generic 1-dimensional Smoluchowski's coagulation equation [32]

$$\dot{n}_k(t) = \frac{1}{2} \sum_{k=i+j} \kappa(i, j) n_i n_j - \sum_i \kappa(i, k) n_i n_k. \quad (10)$$

The vectorial representation of the multi-species system smoothly generalizes aggregation into a vector addition

$$\mathbf{k} = \mathbf{i} + \mathbf{j} \quad (11)$$

to allow particles in different species to connect together. It follows that now we can write down the aggregation term in the master equations almost exactly the same as before:

$$\sum_{\mathbf{k}=\mathbf{i}+\mathbf{j}} \kappa(\mathbf{i}, \mathbf{j}) n_{\mathbf{i}} n_{\mathbf{j}}, \quad (12)$$

where $\kappa(\mathbf{i}, \mathbf{j})$ is the generic kernel function of aggregation. The summation here accounts for all possible combinations of \mathbf{i} and \mathbf{j} . It is a shorthand notation of a multiple summation on each of the D species:

$$\sum_{\substack{k_1=i_1+j_1 \\ 0 \leq i_1 \leq k_1-1 \\ 0 \leq j_1 \leq k_1-1}} \sum_{\substack{k_2=i_2+j_2 \\ 0 \leq i_2 \leq k_2-1 \\ 0 \leq j_2 \leq k_2-1}} \cdots \sum_{\substack{k_D=i_D+j_D \\ 0 \leq i_D \leq k_D-1 \\ 0 \leq j_D \leq k_D-1}} \kappa(\mathbf{i}, \mathbf{j}) n_{\mathbf{i}} n_{\mathbf{j}}. \quad (13)$$

Comparing this with the aggregation term in Eq. (10), this extension in dimensionality becomes apparent. Now the master equations for multiple species can be readily obtained from generalizing Eq. (10) into

$$\dot{n}_{\mathbf{k}}(t) = \frac{1}{2} \sum_{\mathbf{k}=\mathbf{i}+\mathbf{j}} \kappa(\mathbf{i}, \mathbf{j}) n_{\mathbf{i}} n_{\mathbf{j}} - \sum_{\mathbf{i}} \kappa(\mathbf{i}, \mathbf{k}) n_{\mathbf{i}} n_{\mathbf{k}}. \quad (14)$$

Due to the nice mathematical properties of the special product kernel $\kappa(\mathbf{i}, \mathbf{j}) = \mathbf{i} \cdot \mathbf{j}$ and its close connections to random graph theory [45, 46] – as well as the fact that a product kernel is consistent with empirical data, as referenced in the main paper – our previous 1-D model is constructed from a binary aggregation model with product kernel. Indeed, the product can be interpreted as aggregation rates due to pairwise interactions on particle level, and there are $\mathbf{i} \cdot \mathbf{j}$ possible interactive pairs. Its natural extension in multi-species models is a dot product:

$$\kappa(\mathbf{i}, \mathbf{j}) = \mathbf{i} \cdot \mathbf{j}. \quad (15)$$

However, this definition does not satisfy our assumption in that it does not admit cross-species aggregations – for example, a cluster (2, 0) can never merge with another cluster (0, 3), and so the system is, at the end of the day, still a decoupled system of multiple species, and this high-dimensional construction is simply a redundant bundle of D 1-dimensional master equations. Furthermore, if we introduce heterogeneity parameter $F(t)$ under the “dot product kernel”, since it is just a scalar multiplier, this means that all the species have to adhere to the same underlying interaction mechanism. In other words, there is no heterogeneity between species.

Fixing these issues only requires some simple tweaks. Since we want cross-species interactions to be possible and that each pair of species should be able to obey different heterogeneous parameters, we simply insert a metric tensor between the two vectors:

$$\kappa(\mathbf{i}, \mathbf{j}) = \mathbf{i}^T \mathbf{F} \mathbf{j}. \quad (16)$$

Due to the symmetric assumption of aggregation, that cluster A aggregating upon B is identical to the opposite, the tensor \mathbf{F} is naturally symmetric. Each non-zero entry $F_{\alpha\beta}$ indicates an existing pair of interactive species α and β , and its value is simply the mean-field heterogeneous parameter. We call \mathbf{F} the heterogeneous matrix. It measures the collective chemistry of the aggregating system.

Not only does it satisfy the mathematical formalism at meso-scale, \mathbf{F} can also be motivated and defined just like its 1-D counterpart as in Ref. [36]. We assume that a token p of species $\alpha = 1, \dots, D$ has an arbitrary number of microscopic traits represented with vector $\vec{y}_{p,\alpha}(t)$, which defines its heterogeneous attributes. We call it the *character* of the particle. Since we are studying aggregation, we hope to quantify how heterogeneity affects fusion rates. Mathematically, this means defining species-dependent functions $S_{\alpha\beta}(\vec{y}_{1;\alpha}, \vec{y}_{2;\beta}, t)$, named *similarity*, which serves as a multiplier of the aggregation rate of particles $\vec{y}_{1;\alpha}$ and $\vec{y}_{2;\beta}$. The form of $S_{\alpha\beta}(\vec{y}_{1;\alpha}, \vec{y}_{2;\beta}, t)$ determines the “chemistry” of aggregation: *homophily* (similar particles are more likely to aggregate), *heterophily* (similar particles are less likely to aggregate), or neutral, in which case $S_{\alpha\beta}$ is constant, among other, more complex choices. We further define the system-wide character distribution $q(\vec{y}, t)$ – note that it can be time-dependent in principle. Averaging over the system then defines $F_{\alpha\beta}(t)$:

$$F_{\alpha\beta}(t) = \int_{\vec{y}_{1;\alpha} \in \mathcal{V}_{\alpha}} \int_{\vec{y}_{2;\beta} \in \mathcal{V}_{\beta}} S_{\alpha\beta}(\vec{y}_{1;\alpha}, \vec{y}_{2;\beta}, t) q(\vec{y}_{1;\alpha}, t) q(\vec{y}_{2;\beta}, t) d\vec{y}_{1;\alpha} d\vec{y}_{2;\beta}, \quad (17)$$

where $\mathcal{V}_{\alpha,\beta}$ is respectively the vector space of the character vectors $\vec{y}_{1;\alpha,2;\beta}$, i.e. the range of all possible characters. This resultant matrix \mathbf{F} is free from microscopic dependence on any particle, and is thus a valid macroscopic variable suitable for our theory.

It follows that we can extend the 1-dimensional master equation

$$\dot{n}_{\mathbf{k}}(t) = \frac{F(t)}{N^2} \sum_{\mathbf{k}=\mathbf{i}+\mathbf{j}} \mathbf{i} \cdot \mathbf{j} n_{\mathbf{i}} n_{\mathbf{j}} - \frac{2F(t)}{N^2} \mathbf{k} \sum_{\mathbf{i}} \mathbf{i} n_{\mathbf{i}} n_{\mathbf{k}} \quad (18)$$

into the following form:

$$\frac{dn_{\mathbf{k}}}{dt} = \frac{1}{N^2} \sum_{\mathbf{k}=i+j} \mathbf{i}^T \mathbf{F} \mathbf{j} n_i n_j - \frac{2}{N^2} \mathbf{k}^T \mathbf{F} \mathbf{N} n_{\mathbf{k}}. \quad (19)$$

In order to simplify the calculations, we rescale the quantities into dimensionless form:

$$\nu_{\mathbf{k}} = \frac{D}{N} n_{\mathbf{k}}, \quad \tau = \frac{2t}{N}. \quad (20)$$

The rescaled master equation then reads

$$\frac{d\nu_{\mathbf{k}}}{d\tau} = \frac{1}{2D} \sum_{\mathbf{k}=i+j} \mathbf{i}^T \mathbf{F} \mathbf{j} \nu_i \nu_j - \mathbf{k}^T \mathbf{F} \left(\frac{N}{N} \right) \nu_{\mathbf{k}}. \quad (21)$$

Adding a generic term $g(\mathbf{k}, \tau)$ that represents other existent interactions, e.g. multi (3 and above)-body aggregation and fission, gives Eq. (1) in the main paper. The $D \times D$ matrix \mathbf{F} is a D -dimensional extension of the mean-field heterogeneous parameter $F(t)$ in [36]. Its entries $F_{\alpha\beta}$ represent the heterogeneity of aggregation between species- α and β particles, and therefore each entry can be obtained by the same mean-field method as in the 1-dimensional theory. As before, our theory permits dynamic $N_{\alpha}(t)$ and $\mathbf{F}(t)$, but our main paper focuses on the intriguing physics with them being held constant.

B. Generating functions, moment tensors & generative PDEs

After extending the two important variables \mathbf{k} and $n_{\mathbf{k}}$ for multi-species aggregation, we follow by defining the multi-species equivalence of the generating functions. The first generating function \mathcal{D} is defined by

$$\mathcal{D}(\mathbf{x}, \tau) \equiv \sum_{\mathbf{k}} n_{\mathbf{k}} e^{-\mathbf{k} \cdot \mathbf{x}}. \quad (22)$$

This defines a Laplace transformation between $\mathcal{D}(\mathbf{x}, t)$ and $n_{\mathbf{k}}(t)$. Note that the reciprocal space of size profile \mathbf{k} , where \mathbf{x} lives, is now also a D -dimensional vector space as well, similar to \mathbf{k} -space. The duality between the generating function and $n_{\mathbf{k}}(t)$ found in 1-species systems still holds. However, the second generating function is now vectorial:

$$\mathcal{E}(\mathbf{x}, t) \equiv -\nabla \mathcal{D}(\mathbf{x}, t) = \sum_{\mathbf{k}} \mathbf{k} n_{\mathbf{k}} e^{-\mathbf{k} \cdot \mathbf{x}}. \quad (23)$$

By taking $\mathbf{x} = \mathbf{0}$ we can obtain the first moment, also a vector:

$$\mathbf{M}_1 = \mathcal{E}(\mathbf{0}, t) = \sum_{\mathbf{k}} \mathbf{k} n_{\mathbf{k}} \equiv N. \quad (24)$$

It still measures the number of particles – only now its components correspond to different species. Generally for higher orders of moment functions, they all become tensorial, as we can see below using suffix notation:

$$(\mathbf{M}_n)_{\alpha_1 \dots \alpha_n} = (-1)^n \partial_{\alpha_1} \dots \partial_{\alpha_n} \mathcal{D}(x_{\alpha}, t), \quad \alpha_{1,2,\dots,n} = 1, 2, \dots, D. \quad (25)$$

We will take a closer look at the second moment tensor and its dynamics later – as in 1-dimensional systems it governs the dynamics of cohesive unit formation. In this Section we focus on the generating functions and their corresponding generative PDEs. We further define the rescaled generating functions

$$\delta(\mathbf{x}, \tau) = \frac{D}{N} \mathcal{D}(\mathbf{x}, \tau), \quad \varepsilon_{\alpha}(\mathbf{x}, \tau) = \frac{D}{N} \mathcal{E}_{\alpha}(\mathbf{x}, \tau) \quad (26)$$

as direct Laplace transformations of $\nu_{\mathbf{k}}(\tau)$ and $k_{\alpha} \nu_{\mathbf{k}}(\tau)$ respectively, such that

$$\delta(\mathbf{x}, \tau) = \sum_{\mathbf{k}} \nu_{\mathbf{k}} e^{-\mathbf{k} \cdot \mathbf{x}}, \quad \varepsilon_{\alpha}(\mathbf{x}, \tau) = \sum_{\mathbf{k}} k_{\alpha} \nu_{\mathbf{k}} e^{-\mathbf{k} \cdot \mathbf{x}} = -\partial_{\alpha} \delta(\mathbf{x}, \tau). \quad (27)$$

The generative equation then follows from Laplace transforming Eq. (21):

$$\frac{\partial \delta}{\partial \tau} = \frac{1}{2D} F_{\alpha\beta} (\varepsilon_\alpha - 2\nu_\alpha) \varepsilon_\beta, \quad (28)$$

where we define constant vector

$$\nu_\alpha = 1 \quad \forall \alpha = 1, \dots, D. \quad (29)$$

One more partial derivative in x_α yields

$$\frac{\partial \varepsilon_\alpha}{\partial \tau} + \frac{1}{D} F_{\beta\gamma} (\varepsilon_\beta - \nu_\beta) \partial_\alpha \varepsilon_\gamma = 0. \quad (30)$$

This is a direct D -dimensional generalization of the inviscid Burgers' equation with shear interactions added. Since by definition,

$$\partial_\alpha \varepsilon_\gamma = \sum_{\mathbf{k}} \partial_\alpha k_\gamma \nu_{\mathbf{k}} e^{-\mathbf{k} \cdot \mathbf{x}} = - \sum_{\mathbf{k}} k_\alpha k_\gamma \nu_{\mathbf{k}} e^{-\mathbf{k} \cdot \mathbf{x}} = \partial_\gamma \varepsilon_\alpha, \quad (31)$$

Eq. (30) can be rewritten exactly as:

$$\frac{\partial \varepsilon_\alpha}{\partial \tau} + \frac{1}{D} F_{\beta\gamma} (\varepsilon_\beta - \nu_\beta) \partial_\gamma \varepsilon_\alpha = 0. \quad (32)$$

As in Eq. (21), adding in the transformed term of $g(\mathbf{k}, \tau) \mathbf{k}$ gives the general form of the generative equation (Eq. (2)) in the main paper.

Eq. (32) is analytically solvable with the characteristics method, just like its 1-D prototype. We can write down the characteristic equations:

$$\frac{dx_\alpha}{d\tau} = \frac{F_{\alpha\beta}}{D} (\varepsilon_\beta - \nu_\beta), \quad (33)$$

where we use the fact that $F_{\alpha\beta}$ is symmetric. For analyticity we assume $F_{\alpha\beta}$ to be time-independent. This can then be solved by

$$x_\alpha(\tau) = \frac{F_{\alpha\beta}}{D} (\varepsilon_\beta - \nu_\beta) \tau + f_\alpha(\boldsymbol{\varepsilon}), \quad (34)$$

where f_α is to be determined by initial condition. With an all-monomer initial condition

$$\varepsilon_\alpha(\mathbf{x}, \tau = 0) = e^{-x_\alpha}, \quad (35)$$

we have

$$x_\alpha(0) = -\ln \varepsilon_\alpha = f_\alpha, \quad (36)$$

and the implicit yet exact solution to Eq. (32) is

$$\ln \varepsilon_\alpha = \frac{F_{\alpha\beta}}{D} (\varepsilon_\beta - \nu_\beta) \tau - x_\alpha \quad (37)$$

Finally, we take $x_\alpha = 0$ to look at behaviors of cohesive unit formation. It follows that

$$\begin{aligned} \frac{F_{\alpha\beta}}{D} (\varepsilon_\beta - \nu_\beta) \tau - \ln \varepsilon_\alpha &= 0 \\ \Rightarrow \varepsilon_\alpha &= e^{-\sum_\beta F_{\alpha\beta} (1 - \varepsilon_\beta) \tau / D}, \end{aligned} \quad (38)$$

where in the last equality we abandon the summation convention. This is Eq. (3) in the main paper after substituting $G_\alpha(\tau) = 1 - \varepsilon_\alpha(0, \tau)$. For reference we right down the solution to cohesive unit formation for 1-species systems, the derivations of which can be found in [36]:

$$\varepsilon = e^{-F(1-\varepsilon)\tau}. \quad (39)$$

We can see that Eq. (38) is a direct generalization of Eq. (39) – each cross-species interaction simply corresponds to an additional multiplicative factor $e^{-F_{\alpha\beta}(1-\varepsilon_\beta)\tau/D}$. The denominator D accounts for the fact that the number of particles in each species is now $1/D$ of the total particles.

C. Dynamics of the second moment tensor

In 1-D systems we know that divergence of the second moment M_2 corresponds to onset of cohesive unit. However, for multi-species systems, the second moment is elevated into a rank-2 tensor. Fortunately, its dynamics is still rather straightforward, as we will see below. We first take one more partial derivative *wrt* x_α on Eq. (32) to obtain

$$\partial_\tau \partial_\beta \varepsilon_\alpha + \frac{F_{\gamma\delta}}{D} [\partial_\beta \varepsilon_\gamma \partial_\delta \varepsilon_\alpha + (\varepsilon_\gamma - \nu_\gamma) \partial_\beta \partial_\delta \varepsilon_\alpha] = 0. \quad (40)$$

Then we set $x_\alpha = 0$, $\forall \alpha = 1, \dots, D$, and by rescaling M_2 the same way as rescaling the generating functions

$$(m_2)_{\alpha\beta} = -\partial_\alpha \varepsilon_\beta = -\partial_\beta \varepsilon_\alpha, \quad (41)$$

we can obtain its governing ODE:

$$\frac{dm_2}{d\tau} = \frac{1}{D} m_2 F m_2, \quad (42)$$

This is a matrix Riccati equation. To solve it we start by left-multiplying the inverse matrix m_2^{-1} to obtain

$$m_2^{-1} \frac{dm_2}{d\tau} = \frac{1}{D} F m_2. \quad (43)$$

Since

$$\frac{d}{d\tau} (m_2^{-1} m_2) = m_2^{-1} \frac{dm_2}{d\tau} + \frac{dm_2^{-1}}{d\tau} m_2 = 0, \quad (44)$$

we have

$$-\frac{dm_2^{-1}}{d\tau} m_2 = \frac{1}{D} F m_2, \quad (45)$$

and thus

$$m_2^{-1} = m_2^{-1}(0) - F \frac{\tau}{D}. \quad (46)$$

As usual we consider the all-monomer initial condition:

$$m_2^{-1}(0) = \mathbb{I}. \quad (47)$$

It follows that

$$m_2^{-1} = \mathbb{I} - \frac{1}{D} F \tau. \quad (48)$$

What follows immediately is the time-to-cohesion τ_g , at which point the determinant of m_2 diverges, i.e.

$$\det(m_2^{-1}(\tau_g)) = 0, \quad (49)$$

a D 'th order polynomial equation. Solutions for $D = 2$ are straightforward and will be presented shortly in Section IV. Analytic solutions for $D = 3$ exist but are highly complicated – some interesting results that can be obtained analytically will be discussed in Section V. For $D > 3$ solutions are generally numerical only.

III. AGGREGATION THEORY FOR GENERAL MULTI-SPECIES SYSTEMS

In this Section we formulate the exact mathematics describing the onsets of cohesive units. We begin with writing down the inverse of second moment, m_2^{-1} , explicitly:

$$m_2^{-1} = \begin{pmatrix} 1 - F_{11}\tau/D & -F_{12}\tau/D & \cdots & -F_{1D}\tau/D \\ -F_{21}\tau/D & 1 - F_{22}\tau/D & \cdots & -F_{2D}\tau/D \\ \vdots & \vdots & \ddots & \vdots \\ -F_{D1}\tau/D & -F_{D2}\tau/D & \cdots & 1 - F_{DD}\tau/D \end{pmatrix}. \quad (50)$$

We extract a common factor $-\tau/D$ out of the matrix bulk:

$$\mathbf{m}_2^{-1} = -\frac{\tau}{D} \begin{pmatrix} F_{11} - D/\tau & F_{12} & \cdots & F_{1D} \\ F_{21} & F_{22} - D/\tau & \cdots & F_{2D} \\ \vdots & \vdots & \ddots & \vdots \\ F_{D1} & F_{D2} & \cdots & F_{DD} - D/\tau \end{pmatrix} \quad (51)$$

and define the new matrix as

$$\omega = \begin{pmatrix} F_{11} - D/\tau & F_{12} & \cdots & F_{1D} \\ F_{21} & F_{22} - D/\tau & \cdots & F_{2D} \\ \vdots & \vdots & \ddots & \vdots \\ F_{D1} & F_{D2} & \cdots & F_{DD} - D/\tau \end{pmatrix} = -\frac{D}{\tau} \mathbf{m}_2^{-1}. \quad (52)$$

Note that ω can be written as

$$\omega(\tau_g) = \mathbf{F} - \frac{D}{\tau_g} \mathbb{I}. \quad (53)$$

From Eq. (49) we can deduce that

$$\det(\omega(\tau_g)) = \left(-\frac{D}{\tau_g}\right)^D \det(\mathbf{m}_2^{-1}(\tau_g)) = 0. \quad (54)$$

By combining Eqs. (53, 54), we can see that Eq. (54) is in fact the *characteristics equation* of the symmetric matrix \mathbf{F} , written out explicitly as

$$\left| \mathbf{F} - \frac{D}{\tau_g} \mathbb{I} \right| = 0, \quad (55)$$

and $\lambda_\mu \equiv D/(\tau_g)_\mu$ are its eigenvalues. In other words, solutions to time-to-cohesion are the inverses of the eigenvalues of \mathbf{F} . But we stress that this does not mean that all solutions are guaranteed to be physical. For 1-species systems, we know that the onset time is the inverse of scalar F . This significant D -dimensional result is its natural extension.

The above result also means that the multi-species fusion problem is essentially a diagonalization problem of the \mathbf{F} matrix. We define the diagonalization of matrix \mathbf{F} as

$$\Lambda = \text{diag}(\lambda_1, \dots, \lambda_D), \quad (56)$$

and denote the corresponding eigenvector of λ_μ as $\mathbf{x}^{(\mu)}$. They satisfy

$$(\mathbf{F} - \lambda_\mu \mathbb{I}) \mathbf{x}^{(\mu)} = \mathbf{0}. \quad (57)$$

Because \mathbf{F} is symmetric, the eigenvectors are mutually orthogonal, i.e. $\mathbf{x}^{(\mu)} \cdot \mathbf{x}^{(\nu)} = \delta_{\mu\nu}$. Consequently, $\{\mathbf{x}^{(\mu)}\}$ form an orthonormal basis that spans the D -dimensional abstract space of \mathbf{x} . Moreover, the basis vectors of its dual space of size profile $\{\mathbf{k}^{(\mu)}\}$ must satisfy, by definition,

$$\mathbf{k}^{(\mu)} \cdot \mathbf{x}^{(\nu)} = \delta_{\mu\nu}. \quad (58)$$

These $\{\mathbf{k}^{(\mu)}\}$ basis vectors are physically significant – their components represent the relative **compositions** of each species at the onset of cohesive unit, and thus we call them the **eigendirections** for cohesive unit formation. For convenience we sometimes call $\mathbf{x}^{(\mu)}$'s as eigendirections also, since they are related to $\mathbf{k}^{(\mu)}$ simply by an inverse. In order to show why they represent cohesive unit compositions, we return to Eq. (28). Obviously the generative equation is frame-independent since all the terms in Eq. (28) are scalars. Hence, we are free to transform it into the eigenbasis of \mathbf{F} . In the rotated frame, Eq. (32), i.e. the generalized Burgers' equation, now reads

$$\frac{\partial \varepsilon'_\mu}{\partial \tau} + \frac{1}{D} \sum_{\nu=1}^D \lambda_\nu (\varepsilon'_\nu - \iota'_\nu) \partial_\nu \varepsilon'_\mu = 0, \quad (59)$$

where in this shorthand notation, $\partial_\mu = \partial/\partial x'_\mu$, $\iota = \sum_{\mu=1}^D \iota'_\mu \mathbf{k}^{(\mu)}$ and $\varepsilon = \sum_{\mu=1}^D \varepsilon'_\mu \mathbf{k}^{(\mu)}$. Now that the diagonal matrix Λ is the heterogeneity rate matrix under this frame, it means that these D linear combinations of species,

i.e. the “bundled” species $\mathbf{k}^{(\mu)}$ ’s, are completely decoupled. This in turn means that as long as the initial condition contains only these “bundled-up” clusters and their aggregates, i.e. $\propto \mathbf{k}^{(\mu)}$ (equivalent to “pure” clusters under this rotated frame), then we always have $\partial_\nu \varepsilon'_\mu = 0$ if $\mu \neq \nu$, and hence, (no sum)

$$\frac{\partial \varepsilon'_\mu}{\partial \tau} + \frac{\lambda_\mu}{D} (\varepsilon'_\mu - \iota'_\mu) \partial_\mu \varepsilon'_\mu = 0. \quad (60)$$

Physically this means that cohesive unit formation must retain these species bundles, i.e. occurring along these **eigendirections**. Therefore, the (inverses of) eigenvectors of F do indeed yield the cohesive unit composition at onset!

However, there remains the problem of physicality – all of $\{\mathbf{k}^{(\mu)}\}$ are not necessarily physical eigendirections, since in principle there can be negative components in $\mathbf{k}^{(\mu)}$, while we obviously do not allow for negative number of particles in a physical cluster. Fortunately, this is resolved by the *Perron-Frobenius theorem*, which states that for an irreducible non-negative matrix, its largest eigenvalue corresponds to an eigenvector whose components are all positive. By assumption, all entries of F represent aggregation rates ($F_{\alpha\beta} \geq 0$), so it must be non-negative. In order to apply the theorem to F we need to first investigate the conditions for its irreducibility.

To begin with, we recall the definition of matrix irreducibility. A matrix M is *reducible* if there exists a *permutation matrix* P such that matrix PMP^{-1} is block upper triangular, i.e. it can be written into the form

$$PMP^{-1} = \begin{pmatrix} A & B \\ 0 & C \end{pmatrix} \quad (61)$$

for some A, B, C . However, a more straightforward definition to apply to our system is the following graphical one. Consider the matrix M as a graph representation. If the graph is connected, M is irreducible. For an asymmetric M , it represents a directed graph, and the connection requirement is such that starting from every vertex on the graph, it is possible to reach all the others. In other words, there cannot be sinks or sources. For symmetric matrices like F , on the contrary, the condition is more straightforward – since it represents an undirected graph, simple connection of all vertices suffices. Therefore, we are able to draw the two following conclusions from this graphical perspective:

1. There must be at least $2(D - 1)$ non-zero $F_{\alpha\beta}$ values for the $D \times D$ matrix F to be irreducible.
2. F is reducible iff it is block diagonal (or can be permuted into a block diagonal form).

The second point above is very important – it follows that, after relabelling the species appropriately, we must be able to write any reducible F into the following form:

$$F = \begin{pmatrix} F_1 & 0 & & 0 \\ 0 & F_2 & & 0 \\ & & \ddots & \\ 0 & & & F_{d-1} & 0 \\ & & & 0 & F_d \end{pmatrix}, \quad (62)$$

for some $2 \leq d \leq D$, where all $F_s, \forall s = 1, 2, \dots, d$ are irreducible. By doing this we have split the system into d decoupled subsystems, each of which irreducible, i.e. fully coupled. We can further extend the range of d to include the trivial case $d = 1$ – it simply represents a fully-coupled system in its own right.

Now we are ready to apply the Perron-Frobenius theorem to all F_s ’s. Each of these matrices must have a maximum eigenvalue, which we can freely relabel as $\lambda_1^{(s)}$, and its corresponding eigenvector $\mathbf{x}_1^{(s)}$ must have all its components positive. Consequently, its dual vector $\mathbf{k}_1^{(s)}$ is a physical eigendirection. Since $\mathbf{x}_1^{(s)}$ is orthogonal to all the other eigenvectors due to symmetric matrix F_s , we can further deduce that all the other eigenvectors must contain at least one negative components (they cannot all be negative of course), and thus unphysical for cohesive unit formation. We can conclude that for each irreducible submatrix F_s , there exists and only exists **1 physical eigendirection** for cohesive unit formation, $\mathbf{k}_1^{(s)}$. Its corresponding physical onset time $\tau_g^{(s)}$, on the other hand, is given by the **largest eigenvalue** of F_s , as

$$\tau_g^{(s)} = \frac{D}{\lambda_1^{(s)}}. \quad (63)$$

For the whole D -species system, there are then d separate and independent onsets of cohesive units, and their respective onset times are $D/\lambda_1^{(s)}$. This exactly agrees with our lower-dimensional results, where decoupled systems aggregate separately. Moreover, this successfully explains why turning on inter-species aggregation instantaneously makes larger roots of τ_g unphysical – it is really that their corresponding eigendirections rotate into unphysical (negative) realms.

In the next few Sections we will focus our discussions on the 2-species and 3-species scenarios to see how the complexity increases as the number of species D increases.

IV. SCENARIO 1: 2-SPECIES AGGREGATION AND COHESIVE UNIT FORMATION

For 2-species aggregation, we take $D = 2$ and the solutions of $\varepsilon_{1,2}$ can be obtained from Eq. (38) to be

$$\varepsilon_\alpha = e^{-\sum_{\beta=1}^2 F_{\alpha\beta}(1-\varepsilon_\beta)\tau/2}, \quad i = 1, 2. \quad (64)$$

In this Section, we shall discuss in depth the cohesion behaviors on and after onset from the dynamics of ε_α and \mathbf{m}_2 , the aforementioned second moment tensor.

A. Time-to-cohesion

We begin with some notational convention: we write the diagonal entries of \mathbf{F} as f_α and the off-diagonal entries $\epsilon_{\alpha\beta}$. For $D = 2$, since the only two off-diagonal elements are identical, we further denote that $\epsilon_{12} = \epsilon_{21} = \epsilon$. Then, from Eq. (48), we have

$$\mathbf{m}_2^{-1} = \frac{1}{2} \begin{pmatrix} 1 - f_1\tau/2 & -\epsilon\tau/2 \\ -\epsilon\tau/2 & 1 - f_2\tau/2 \end{pmatrix} \quad (65)$$

and

$$\begin{aligned} \det(\mathbf{m}_2^{-1}) &= (1 - f_1\tau/2)(1 - f_2\tau/2) - \epsilon^2\tau^2/4 \\ &= \frac{1}{4}(f_1f_2 - \epsilon^2)\tau^2 - \frac{1}{2}(f_1 + f_2)\tau + 1. \end{aligned} \quad (66)$$

Therefore, the time-to-cohesion τ_g satisfies the following quadratic equation

$$(f_1f_2 - \epsilon^2)(\tau_g/2)^2 - (f_1 + f_2)(\tau_g/2) + 1 = 0, \quad (67)$$

and its two roots are

$$\tau_g^{(1,2)} = \frac{(f_1 + f_2) \mp \sqrt{(f_1 - f_2)^2 + 4\epsilon^2}}{(f_1f_2 - \epsilon^2)}. \quad (68)$$

This appears in the main paper as Eq. (5).

Now let's look into the properties of τ_g and \mathbf{m}_2 , especially their dependence on the parameters $f_{1,2}$ and ϵ and their underlying physical implications. First, we note that the two roots of Eq. (67), as shown in Eq. (68), are always real. Within this 3-D parameter space, it is physically intriguing and mathematically elementary to inspect the relative value of cross-species interaction ϵ against the intra-species interactions $f_{1,2}$. For this matter we fix $f_{1,2}$. A changing ϵ only alters the quadratic coefficient of $\det(\mathbf{m}_2^{-1})(\tau)$ – more specifically, $\tau_g^{(1,2)}$ is determined by ϵ compared with $\sqrt{f_1f_2}$, i.e. the geometric average of f_1 and f_2 . For small $\epsilon < \sqrt{f_1f_2}$, both roots are positive. As ϵ increases, the smaller root $\tau_g^{(1)}$ contracts while the larger one $\tau_g^{(2)}$ diverges. Just at the geometric average $\epsilon = \sqrt{f_1f_2}$, the quadratic coefficient cancels, $\det(\mathbf{m}_2^{-1})(\tau)$ becomes linear in τ , and there is one sole root, positive. For relatively stronger inter-species interaction $\epsilon > \sqrt{f_1f_2}$ only the larger root $\tau_g^{(2)}$ is now positive, i.e. the physical solution, and it decreases further as ϵ continues increasing. As $\epsilon \rightarrow \infty$, the onset time $\tau_g \rightarrow 0$. The trend above is illustrated in Fig. 4(a) in the main paper, where $\tau_g^{(1,2)}$ are plotted against ϵ with $f_{1,2}$ fixed at 1.2 and 0.4, respectively. Meanwhile, Fig. 5 below plots the shapes of the quadratics $\det(\mathbf{m}_2^{-1})(\tau)$ at different ϵ values and the same fixed values of $f_{1,2}$.

Now that the math is clear, we return to Section III for its physical interpretation. At $\epsilon = 0$, \mathbf{F} is diagonal, and hence trivially reducible into two decoupled and independent 1-D subsystems. In this case, the two roots $\tau_g^{(1,2)}$ are both physical, corresponding to the two separate onsets of cohesive units. From Eq. (68) we know that $\tau_g^{(1)} = 2/f_1$ and $\tau_g^{(2)} = 2/f_2$, and $2/\tau_g^{(1,2)}$ are exactly the two eigenvalues (i.e. diagonal entries) of \mathbf{F} . Furthermore, the two eigenvectors of $\mathbf{F}(\epsilon = 0)$ are trivially $(1, 0)$ and $(0, 1)$, exactly the two physical eigendirections (two separate pure cohesive units). This verifies our general theory. Once we turn on $\epsilon > 0$, the smallest positive root ($\tau_g^{(1)}$ for $\epsilon < \sqrt{f_1f_2}$ and $\tau_g^{(2)}$ for $\epsilon > \sqrt{f_1f_2}$) always corresponds to the largest eigenvalue of \mathbf{F} , and hence the sole physical onset. When $\epsilon < \sqrt{f_1f_2}$, the other positive root $\tau_g^{(2)}$ is not physically observed in the system, hence *virtual*. Its increasing value against ϵ , as shown in Fig. 4(a), however, exhibits a latency of the slower-aggregating species due to the increasing tendency of these particles to participate the mixed onset, precisely due to the increasing inter-species interaction ϵ . We shall

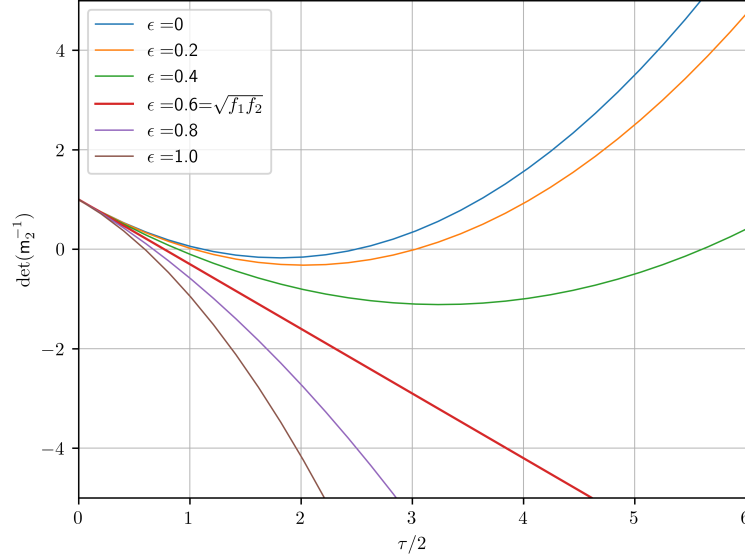


FIG. 5. $\det(\mathbf{m}_2^{-1})(\tau)$ at 6 different ϵ values, with $f_{1,2}$ fixed at 0.9 and 0.4, respectively.

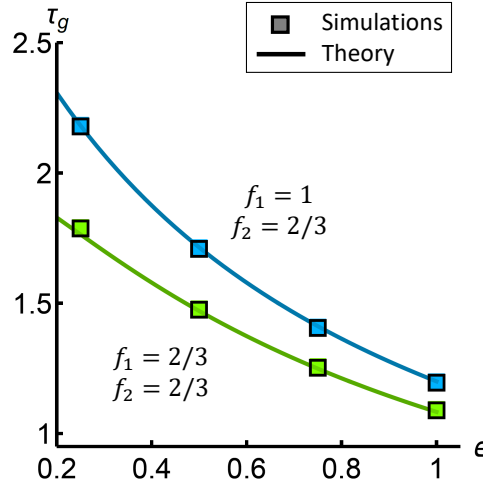


FIG. 6. Time-to-cohesion versus the parameter ϵ , which shows the very good agreement between our analytic solutions and full simulation results.

further examine our theory in the next Section as we solve for the exact cohesive unit composition at onset time for 2 species – there we shall see that the corresponding eigendirection to $\tau_g^{(2)}$ does indeed contain exactly 1 negative component, hence virtual. Lastly, at $\epsilon = \sqrt{f_1 f_2}$ the larger root becomes divergent, and $\epsilon > \sqrt{f_1 f_2}$ there is only one positive root – the negative one is *unphysical*. This is due to the fact that under these conditions, particles are more likely to aggregate across species instead of within.

Our analytical results are also compared with simulations and Fig. 6 shows very good agreement.

B. Composition of the cohesive unit at onset

After looking at the determinant of \mathbf{m}_2 , we now turn to its components. Qualitatively, the second moment near the onset time of cohesion should provide a measurement of cohesive unit composition around the onset, i.e. the proportions of two species in the cohesive unit. This is not hard to see qualitatively – due to its quadratic nature, the contribution from the largest cluster (the “*quasi-cohesive unit*”) becomes dominant near onset time. Consequently, it should be a reasonable approximation that, near onset time,

$$\mathbf{m}_2 \sim A \begin{pmatrix} K_1^2 & K_1 K_2 \\ K_1 K_2 & K_2^2 \end{pmatrix}, \quad (69)$$

where K_1, K_2 are the respective proportions of type-1,2 particles in the “quasi-cohesive unit”, and A is a very large factor ($\sim O(N)$) that accounts for the almost-divergent magnitude of \mathbf{m}_2 .

It turns out that Eq. (69) is more than an approximation. It is possible to derive it directly from the matrix components at onset time. But they are all singular then – so how can we extract any other useful information than divergence? Our way around this is to extract out a common factor $1/\Delta$. The denominator $\Delta = \det(\mathbf{m}_2^{-1})$, i.e. *the* cause of divergence. We can then define a divergence-free matrix

$$\mu = \begin{pmatrix} 1 - f_2\tau/2 & \epsilon\tau/2 \\ \epsilon\tau/2 & 1 - f_1\tau/2 \end{pmatrix}, \quad (70)$$

such that

$$\mathbf{m}_2 = \frac{1}{\Delta} \mu. \quad (71)$$

Now we examine the entries of μ at onset and compare them with Eq. (69). For $f_1 f_2 \neq \epsilon^2$, at onset time, we plug in $\tau_g^{(1)}$ found in Eq. (68) and obtain

$$\begin{aligned} \mu_g^{(11)} &= 1 - f_2 \frac{(f_1 + f_2) - \sqrt{(f_1 - f_2)^2 + 4\epsilon^2}}{2(f_1 f_2 - \epsilon^2)} \\ \mu_g^{(12)} &= \epsilon \frac{(f_1 + f_2) - \sqrt{(f_1 - f_2)^2 + 4\epsilon^2}}{2(f_1 f_2 - \epsilon^2)} \\ \mu_g^{(22)} &= 1 - f_1 \frac{(f_1 + f_2) - \sqrt{(f_1 - f_2)^2 + 4\epsilon^2}}{2(f_1 f_2 - \epsilon^2)}. \end{aligned}$$

Note that these expressions are homogeneous in terms of $f_{1,2}$ and ϵ , so we can actually write them in terms of two variables only:

$$\phi_1 = \frac{f_1}{\epsilon}, \quad \phi_2 = \frac{f_2}{\epsilon}. \quad (72)$$

This indicates that when cohesive unit composition is determined by the relative values of these three parameters only. As discussed earlier, their exact values only determine how soon a cohesive unit is formed. The three entries are reduced into

$$\mu_g^{(11)} = \frac{\phi_1 \phi_2 - 2 - \phi_2^2 + \phi_2 \sqrt{(\phi_1 - \phi_2)^2 + 4}}{2(\phi_1 \phi_2 - 1)}, \quad (73)$$

$$\mu_g^{(12)} = \frac{(\phi_1 + \phi_2) - \sqrt{(\phi_1 - \phi_2)^2 + 4}}{2(\phi_1 \phi_2 - 1)}, \quad (74)$$

$$\mu_g^{(22)} = \frac{\phi_1 \phi_2 - 2 - \phi_1^2 + \phi_1 \sqrt{(\phi_1 - \phi_2)^2 + 4}}{2(\phi_1 \phi_2 - 1)}. \quad (75)$$

In order to find their relations, instead of using brute force by working directly on their algebras, we turn to Eq. (65) and note that the inverse of the second moment at onset time of cohesion can simply be written as

$$\mathbf{m}_2^{-1}(\tau_g) = \begin{pmatrix} \mu_g^{(22)} & -\mu_g^{(12)} \\ -\mu_g^{(12)} & \mu_g^{(11)} \end{pmatrix}, \quad (76)$$

and since $\det(\mathbf{m}_2^{-1}(\tau_g)) = 0$, we must have

$$\mu_g^{(22)}\mu_g^{(11)} = \mu_g^{(12)^2}. \quad (77)$$

However, if we return to the definition of the second moment, we have

$$\begin{aligned} \mu_g^{(11)}\mu_g^{(22)} &= \left(\sum_{i=0}^{\infty} \sum_{j=0}^{\infty} i^2 n_{(i,j)} \right) \left(\sum_{i=0}^{\infty} \sum_{j=0}^{\infty} j^2 n_{(i,j)} \right) = \sum_{i=0}^{\infty} \sum_{j=0}^{\infty} i^2 j^2 n_{(i,j)}^2 \\ &\leq \left(\sum_{i=0}^{\infty} \sum_{j=0}^{\infty} i j n_{(i,j)} \right)^2 = \mu_g^{(12)^2}, \end{aligned} \quad (78)$$

where equality can only be reached iff there exists only one cluster profile $\mathbf{k}_0 = (i_0, j_0)$ throughout the system, such that there are no cross terms in the perfect square after the inequality. In the aggregation system, this occurs only at or near cohesion onset, where a giant cluster, i.e. the (quasi-)cohesive unit, dominates the system. In reality, at this point there may well be other smaller clusters in the system, but their contribution to the second moment is negligible compared to the (quasi-)cohesive unit, due to the vast difference in size. Thus, Eq. (77) leads to the following:

$$\mu_g^{(11)} \approx K_1^2, \quad (79)$$

$$\mu_g^{(12)} \approx K_1 K_2, \quad (80)$$

$$\mu_g^{(22)} \approx K_2^2. \quad (81)$$

These expressions confirm our earlier guess, and further specify that $\sqrt{\mu_g^{(11)}}$ and $\sqrt{\mu_g^{(22)}}$ indeed measure the cohesive unit composition. The off-diagonal component $\mu_g^{(12)}$ does not provide extra information apart from being the product $K_1 K_2$. This naturally makes sense, since our mesoscopic model does not distinguish connections by types of aggregating species (intra or inter).

So far we have understood that the proportions of both species, $\eta_{1,2}$, within the cohesive unit around onset time are given by

$$\eta_1 \equiv \frac{\sqrt{\mu_g^{(11)}}}{\sqrt{\mu_g^{(11)}} + \sqrt{\mu_g^{(22)}}}, \quad (82)$$

$$\eta_2 \equiv \frac{\sqrt{\mu_g^{(22)}}}{\sqrt{\mu_g^{(11)}} + \sqrt{\mu_g^{(22)}}} = 1 - \eta_1. \quad (83)$$

Substituting in Eqs. (79-81), we can now express this pair of quantities in terms of parameters $\phi_{1,2}$:

$$\begin{aligned} \eta_1 &= \left(1 + \sqrt{\frac{\mu_g^{(22)}}{\mu_g^{(11)}}} \right)^{-1} \\ &= \left(1 + \sqrt{\frac{\phi_1 \phi_2 - 2 - \phi_1^2 + \phi_1 \sqrt{(\phi_1 - \phi_2)^2 + 4}}{\phi_1 \phi_2 - 2 - \phi_2^2 + \phi_2 \sqrt{(\phi_1 - \phi_2)^2 + 4}}} \right)^{-1}. \end{aligned}$$

We can yet simplify this further. Substituting once more with $\sigma = \phi_1 - \phi_2$, we have

$$\begin{aligned}
\eta_1 &= \left[1 + \sqrt{\frac{\phi_1 (\sqrt{\sigma^2 + 4} - \sigma) - 2}{\phi_2 (\sqrt{\sigma^2 + 4} + \sigma) - 2}} \right]^{-1} \\
&= \left[1 + \sqrt{\frac{(\phi_2 + \sigma) (\sqrt{\sigma^2 + 4} - \sigma) - 2}{\phi_2 (\sqrt{\sigma^2 + 4} + \sigma) - 2}} \right]^{-1} \\
&= \left[1 + \sqrt{1 + \sigma \frac{\sqrt{\sigma^2 + 4} - \sigma - 2\phi_2}{\phi_2 (\sqrt{\sigma^2 + 4} + \sigma) - 2}} \right]^{-1} \\
&= \left[1 + \sqrt{1 + \sigma \left(\sqrt{\sigma^2 + 4} - \sigma \right) \frac{\sqrt{\sigma^2 + 4} - \sigma - 2\phi_2}{4\phi_2 - 2(\sqrt{\sigma^2 + 4} - \sigma)}} \right]^{-1} \\
&= \left[1 + \sqrt{1 - \frac{\sigma}{2} \left(\sqrt{\sigma^2 + 4} - \sigma \right)} \right]^{-1} \\
&= \left[1 + \frac{1}{2} \left(\sqrt{\sigma^2 + 4} - \sigma \right) \right]^{-1} = \frac{2}{\sqrt{\sigma^2 + 4} - \sigma + 2}, \tag{84}
\end{aligned}$$

$$\eta_2 = 1 - \eta_1 = \frac{2}{\sqrt{\sigma^2 + 4} + \sigma + 2}, \tag{85}$$

where in the fourth equality we multiply on both the numerator and the denominator of the fraction inside the square root by $(\sqrt{\sigma^2 + 4} - \sigma)$, and in the sixth equality we find that the expression inside the square root is actually a perfect square. Curiously enough, $\eta_{1,2}$ are monotonic functions in a simple one-parameter space. In other words, the cohesive unit composition at onset depends monotonically on one specific combination of the parameters in the form

$$\sigma = \frac{f_1 - f_2}{\epsilon}. \tag{86}$$

The detailed relations are plotted in Fig. 4(b) in the main paper. They are nicely symmetric, and can also be neatly interpreted: a large f_α corresponds to strong intra-species aggregation for species α , and hence more species- α particles in the cohesive unit, whereas a large ϵ represents strong tendency of inter-species aggregation, and it follows that $\sigma \rightarrow 0$ and therefore comparable number of both species in the cohesive unit.

In the remainder of this section, we will derive the cohesive unit composition at onset using the other two approaches as mentioned in the paper, namely (1). expansion of growth-of-cohesion solution (Eq. (64)) and (2). calculation of the eigendirections. Our goal is to first verify the correctness of Eqs. (84) and (85), and second verify the physical interpretation of eigendirections as cohesive unit compositions.

1. Cohesive unit composition via expansion of growth-of-cohesion solution

We begin with writing out explicitly Eq. (64) as

$$\varepsilon_1 = e^{-[f_1(1-\varepsilon_1)+\epsilon(1-\varepsilon_2)]\tau/2}, \tag{87}$$

$$\varepsilon_2 = e^{-[\epsilon(1-\varepsilon_1)+f_2(1-\varepsilon_2)]\tau/2}. \tag{88}$$

As a reminder they are solutions of Eq. (32) at $x = 0$ for $D = 2$, and thus describe dynamics of cohesive unit formation for species 1 and 2. The plots of $G(\tau) \equiv 1 - (\varepsilon_1 + \varepsilon_2)/2$ are shown in Fig. 3(a) of the main paper. Taking logarithms gives

$$\frac{\tau}{2} = -\frac{\ln \varepsilon_1}{f_1(1-\varepsilon_1) + \epsilon(1-\varepsilon_2)}, \tag{89}$$

$$\frac{\tau}{2} = -\frac{\ln \varepsilon_2}{\epsilon(1-\varepsilon_1) + f_2(1-\varepsilon_2)}. \tag{90}$$

Note that $G_\alpha(\tau) \equiv (1 - \varepsilon_\alpha(\mathbf{0}, \tau))$ represent the proportions of species- α particles within cohesive unit. Here we denote $\varepsilon_\alpha(\mathbf{0}, \tau)$ simply as ε_α for convenience. Hence, we have

$$\frac{\eta_1}{\eta_2} = \frac{1 - \varepsilon_1}{1 - \varepsilon_2}. \quad (91)$$

We equate Eqs. (89) and (90), obtaining

$$(\ln \varepsilon_1)[\varepsilon(1 - \varepsilon_1) + f_2(1 - \varepsilon_2)] = (\ln \varepsilon_2)[f_1(1 - \varepsilon_1) + \varepsilon(1 - \varepsilon_2)]. \quad (92)$$

Around onset of cohesive units, $1 - \varepsilon_\alpha \ll 1$, so we linearize the logarithms and get

$$-(1 - \varepsilon_1)[\varepsilon(1 - \varepsilon_1) + f_2(1 - \varepsilon_2)] = -(1 - \varepsilon_2)[f_1(1 - \varepsilon_1) + \varepsilon(1 - \varepsilon_2)]. \quad (93)$$

Tidying up the equation,

$$\begin{aligned} \varepsilon [(1 - \varepsilon_2)^2 - (1 - \varepsilon_1)^2] &= (f_1 - f_2)(1 - \varepsilon_1)(1 - \varepsilon_2) \\ \Rightarrow \frac{1 - \varepsilon_1}{1 - \varepsilon_2} - \frac{1 - \varepsilon_2}{1 - \varepsilon_1} &= -\frac{f_1 - f_2}{\varepsilon} \equiv -\sigma, \end{aligned} \quad (94)$$

i.e.

$$\left(\frac{\eta_1}{\eta_2}\right)^2 + \sigma \left(\frac{\eta_1}{\eta_2}\right) - 1 = 0. \quad (95)$$

The solution of this quadratic equation is

$$\frac{\eta_1}{\eta_2} = \frac{\sqrt{\sigma^2 + 4} - \sigma}{2}, \quad (96)$$

where we discarded the negative root. Now we check this expression against Eqs. (84, 85):

$$\eta_1 = \frac{2}{\sqrt{\sigma^2 + 4} - \sigma + 2}, \quad \eta_2 = \frac{2}{\sqrt{\sigma^2 + 4} + \sigma + 2},$$

which give

$$\begin{aligned} \frac{\eta_1}{\eta_2} &= \frac{\sqrt{\sigma^2 + 4} - \sigma + 2}{\sqrt{\sigma^2 + 4} + \sigma + 2} \\ &= \frac{(\sqrt{\sigma^2 + 4} - \sigma + 2)(\sqrt{\sigma^2 + 4} + \sigma - 2)}{(\sqrt{\sigma^2 + 4} + \sigma + 2)(\sqrt{\sigma^2 + 4} + \sigma - 2)} \\ &= \frac{\sigma^2 + 4 - (\sigma - 2)^2}{(\sqrt{\sigma^2 + 4} + \sigma)^2 - 4} \\ &= \frac{4\sigma}{2\sigma^2 + 2\sigma\sqrt{\sigma^2 + 4}} = \frac{2}{\sigma + \sqrt{\sigma^2 + 4}} = \frac{\sqrt{\sigma^2 + 4} - \sigma}{2}, \end{aligned} \quad (97)$$

whihc is indeed identical to the result in Eq. (96).

2. Cohesive unit composition as an eigendirection

We finish off this Section by diagonalizing the 2×2 symmetric matrix

$$\mathbf{F} = \begin{pmatrix} f_1 & \varepsilon \\ \varepsilon & f_2 \end{pmatrix}. \quad (98)$$

According to the general theory in Section III, this should yield onset time and composition of the cohesive unit. We denote, as before, the eigenvalues of \mathbf{F} as $\lambda_{1,2}$ and their corresponding eigenvectors $\mathbf{x}^{(1,2)}$. It is not hard to find that

$$\lambda_{1,2} = \frac{(f_1 + f_2) \pm \sqrt{(f_1 - f_2)^2 + 4\varepsilon^2}}{2}, \quad (99)$$

and that

$$\mathbf{x}^{(1)} = \left(2\epsilon, \sqrt{(f_1 - f_2)^2 + 4\epsilon^2} - (f_1 - f_2) \right) \quad (100)$$

$$\mathbf{x}^{(2)} = \left(-2\epsilon, \sqrt{(f_1 - f_2)^2 + 4\epsilon^2} + (f_1 - f_2) \right) \quad (101)$$

(not normalized). We can easily verify that

1. from Eq. (68), onset time

$$\tau_g^{(1)} = \frac{(f_1 + f_2) - \sqrt{(f_1 - f_2)^2 + 4\epsilon^2}}{(f_1 f_2 - \epsilon^2)} = \frac{2}{\lambda_1}, \quad \tau_g^{(2)} = \frac{2}{\lambda_2}. \quad (102)$$

This verifies that the time instants of onset are indeed given by the eigenvalues of \mathbf{F} , and that the first onset correspond exactly to the larger eigenvalue.

2. Both components of $\mathbf{x}^{(1)}$ are positive, and the ratio

$$\frac{k_1^{(1)}}{k_2^{(1)}} = \frac{1/x_1^{(1)}}{1/x_2^{(1)}} = \frac{\sqrt{(f_1 - f_2)^2 + 4\epsilon^2} - (f_1 - f_2)}{2\epsilon} = \frac{\eta_1}{\eta_2} \quad (103)$$

according to Eq. (96). This verifies that $\mathbf{k}^{(1)}$ indeed gives the eigendirection of cohesive unit formation, as stated in Section III.

3. On the contrary, $\mathbf{x}^{(2)}$ precisely has 1 negative component, and it is indeed orthogonal to $\mathbf{x}^{(1)}$. This is therefore an unphysical, or virtual, eigendirection, and $\tau_g^{(2)}$ is thus also virtual.

This concludes our analytic description of a 2-species aggregation system. It serves as a good heuristic example of our general theory.

V. SCENARIO 2: 3-D AGGREGATION AND COHESIVE UNIT FORMATION

In this Section we explore the analytics for 3 species. We again write down \mathbf{m}_2^{-1} explicitly:

$$\mathbf{m}_2^{-1} = \begin{pmatrix} 1 - f_1\tau/3 & -\epsilon_{12}\tau/3 & -\epsilon_{13}\tau/3 \\ -\epsilon_{12}\tau/3 & 1 - f_2\tau/3 & -\epsilon_{23}\tau/3 \\ -\epsilon_{13}\tau/3 & -\epsilon_{23}\tau/3 & 1 - f_3\tau/3 \end{pmatrix}. \quad (104)$$

Now we denote $\gamma = \tau/3$ and $\Delta = \det(\mathbf{m}_2^{-1})$ again, and write down the determinants of the three 2-D submatrices

$$\begin{vmatrix} 1 - f_\alpha\gamma & \epsilon_{\alpha\beta}\gamma \\ \epsilon_{\alpha\beta}\gamma & 1 - f_\beta\gamma \end{vmatrix} \equiv \delta_{\alpha\beta}. \quad (105)$$

Then, taking the inverse of \mathbf{m}_2^{-1} gives

$$\mu = \begin{pmatrix} \delta_{23} & (\epsilon_{23}\gamma)(\epsilon_{13}\gamma) + (\epsilon_{12}\gamma)(1 - f_3\gamma) & (\epsilon_{12}\gamma)(\epsilon_{23}\gamma) + (\epsilon_{13}\gamma)(1 - f_2\gamma) \\ (\epsilon_{23}\gamma)(\epsilon_{13}\gamma) + (\epsilon_{12}\gamma)(1 - f_3\gamma) & \delta_{13} & (\epsilon_{13}\gamma)(\epsilon_{12}\gamma) + (\epsilon_{23}\gamma)(1 - f_1\gamma) \\ (\epsilon_{12}\gamma)(\epsilon_{23}\gamma) + (\epsilon_{13}\gamma)(1 - f_2\gamma) & (\epsilon_{13}\gamma)(\epsilon_{12}\gamma) + (\epsilon_{23}\gamma)(1 - f_1\gamma) & \delta_{12} \end{pmatrix}, \quad (106)$$

where

$$\mathbf{m}_2 = \frac{1}{\Delta}\mu. \quad (107)$$

Since τ_g is now a root of the cubic equation

$$\Delta(\tau_g) = 0 \quad (108)$$

and hence harder to solve, so we do not here pursue an exact evaluation. Nevertheless, we can still check that the diagonal entries, i.e. $\delta_{\alpha\beta}$ here, still measure the composition at onset of cohesion via

$$\delta_{23}\delta_{13} = [(\epsilon_{23}\gamma)(\epsilon_{13}\gamma) + (\epsilon_{12}\gamma)(1 - f_3\gamma)]^2 \quad (109)$$

etc, just like Eq. (77) in 2-D. To write out more explicitly, the proportions of the three species in the cohesive unit are

$$\frac{\sqrt{\delta_{23}}}{\sqrt{\delta_{23}} + \sqrt{\delta_{13}} + \sqrt{\delta_{12}}}, \frac{\sqrt{\delta_{13}}}{\sqrt{\delta_{23}} + \sqrt{\delta_{13}} + \sqrt{\delta_{12}}}, \frac{\sqrt{\delta_{12}}}{\sqrt{\delta_{23}} + \sqrt{\delta_{13}} + \sqrt{\delta_{12}}}, \quad (110)$$

respectively, evaluated at onset time.

A. Evaluating onset time

The cubic nature of Eq. (108) makes its analytic solutions highly complicated, so a numerical evaluation of time-to-cohesion may be a more convenient choice. There are nonetheless some useful analytic results on a cubic equation that we can do without too much sweat, and it turns out that the number of positive roots, and hence the physical roots corresponding to time-to-cohesions, has a not-too-complicated dependency on the relative strengths of the cross-species aggregation rates $\epsilon_{\alpha\beta}$'s.

First, we write down the explicit form of Eq. (108):

$$(f_1\epsilon_{23}^2 + f_2\epsilon_{13}^2 + f_3\epsilon_{12}^2 - f_1f_2f_3 - 2\epsilon_{12}\epsilon_{13}\epsilon_{23})\gamma^3 + (f_1f_2 + f_1f_3 + f_2f_3 - \epsilon_{12}^2 - \epsilon_{13}^2 - \epsilon_{23}^2)\gamma^2 - (f_1 + f_2 + f_3)\gamma + 1 = 0. \quad (111)$$

We start by defining three relative quantities

$$\xi_1 = \frac{\epsilon_{23}^2}{f_2f_3}, \quad \xi_2 = \frac{\epsilon_{13}^2}{f_1f_3}, \quad \xi_3 = \frac{\epsilon_{12}^2}{f_1f_2}. \quad (112)$$

Clearly they measure the relative strengths of the three possible pairs of cross-species aggregation between compared with their respective intra-species aggregations. Then, we can express the cubic and quadratic coefficients A, B in terms of f_α 's and ξ_α 's:

$$A = f_1f_2f_3 \left(\xi_1 + \xi_2 + \xi_3 - 2\sqrt{\xi_1\xi_2\xi_3} - 1 \right) \quad (113)$$

$$B = f_1f_2(1 - \xi_3) + f_1f_3(1 - \xi_2) + f_2f_3(1 - \xi_1). \quad (114)$$

Using Vieta theorem we can discuss the distribution of all three roots, and hence the number of positive roots, as the coefficients takes different signs. Since the linear coefficient $-(f_1 + f_2 + f_3)$ is always negative and the constant term 1 always positive, we deduce that the number of positive roots depends solely on the signs of A and B , as shown in the following table.

A	-	+	+	-
B	+	-	+	-
Nos. of positive roots	3	2	2	1

TABLE I. The number of positive roots dependent upon A and B .

Since by definition $f_{1,2,3} \geq 0$, the signs of A, B depend purely on ξ_α 's. With the use of some simple inequalities we can then find some exact criteria on ξ_α values that determine the number of positive roots. A detailed discussion and quantitative results will soon follow, but first we give a qualitative summary. The general trend is that, as ξ_α 's are tuned up, i.e. as we tune up cross-species aggregation rates, the number of positive roots gradually reduces from 3 to 1. This aligns with what we expect from the 2-D counterpart and shouldn't be too hard to make sense of.

Now comes the lengthy part. The critical value for $\xi_\alpha \equiv \epsilon_{\beta\gamma}^2 / (f_\beta f_\gamma)$ is 1 – it decides whether inter-species aggregation takes over ($\xi_\alpha > 1$) between species β, γ . Hence, we discuss the values of A, B for different values of ξ_α relative to 1. Since ξ_1, ξ_2, ξ_3 are completely symmetric, we hereby assume that $\xi_1 \leq \xi_2 \leq \xi_3$ wlog.

1. When $\xi_1, \xi_2 < 1$ and $\xi_3 > 1$, the value of B looks arbitrary, as its sign depends on ξ_α 's as well as f_α 's. However, the value of A is constrained:

$$\begin{aligned} A &= \xi_1 + \xi_2 + \xi_3 - 2\sqrt{\xi_1\xi_2\xi_3} - 1 \\ &\geq 2\sqrt{\xi_1\xi_2} - 2\sqrt{\xi_1\xi_2\xi_3} + \xi_3 - 1 \\ &= 2\sqrt{\xi_1\xi_2}(1 - \sqrt{\xi_3}) + (\sqrt{\xi_3} + 1)(\sqrt{\xi_3} - 1) \\ &= (\sqrt{\xi_3} + 1 - 2\sqrt{\xi_1\xi_2})(\sqrt{\xi_3} - 1). \end{aligned} \quad (115)$$

Since $\xi_3 > 1$, $\xi_1, \xi_2 < 1$, we have that $\sqrt{\xi_3} > 1$, and $2\sqrt{\xi_1\xi_2} < 2$, and therefore,

$$\sqrt{\xi_3} + 1 - 2\sqrt{\xi_1\xi_2} > 0, \quad \sqrt{\xi_3} - 1 > 0. \quad (116)$$

Thus,

$$A \geq (\sqrt{\xi_3} + 1 - 2\sqrt{\xi_1\xi_2})(\sqrt{\xi_3} - 1) > 0. \quad (117)$$

According to Table I, this corresponds exactly to 2 positive roots. Hence, when there is only one ξ_α above 1 and two below, there are 2 positive roots for τ_g .

2. When $\xi_1 < 1$ and $\xi_2, \xi_3 > 1$, B still takes arbitrary values. Similar to above, it can be shown that $A > 0$ also. Again, this corresponds exactly to 2 positive roots. Hence, when there are only two ξ_α 's above 1 and one below, there are also 2 positive roots for τ_g .

The other two scenarios are a bit more involved.

3. When $\xi_1, \xi_2, \xi_3 < 1$, $B > 0$. The value of A is, however, undetermined, so there can be 3 or 2 positive roots. The exact value depends on the function A . Since ξ_1, ξ_2, ξ_3 are completely symmetric in A , we for now regard ξ_2, ξ_3 as parameters and ξ_1 as the sole variable, in order to determine the condition between ξ_1 and $\xi_{2,3}$ such that A becomes positive/negative. Then A can be seen as a quadratic function with respect to $y_1 \equiv \sqrt{\xi_1}$. We rewrite A as

$$A(y_1) = y_1^2 - 2\sqrt{\xi_2\xi_3}y_1 - (1 - \xi_2 - \xi_3). \quad (118)$$

Clearly $A(y_1)$ has its minimum at $y_1 = \sqrt{\xi_2\xi_3} < 1$, being

$$A(\sqrt{\xi_2\xi_3}) = \xi_2 + \xi_3 - 1 - \xi_2\xi_3 = -(1 - \xi_2)(1 - \xi_3) < 0. \quad (119)$$

This implies that there must exist a range for y_1 , and thus ξ_1 , in which $A < 0$ and there are in turn three positive roots. On the other hand, to decide whether A can ever become positive in this scenario, we need to first check the boundary values $A(0)$ and $A(\sqrt{\xi_2})$ (since $\xi_1 \leq \xi_2$ by assumption). We can see that

$$A(0) = \xi_2 + \xi_3 - 1 \quad (120)$$

depends on the exact values of $\xi_2 + \xi_3$, whereas

$$A(\sqrt{\xi_2}) = (2\xi_2 - 1 - \sqrt{\xi_3})(1 - \sqrt{\xi_3}) < 0, \quad (121)$$

since by definition $\xi_{2,3} < 1$ and by assumption $\xi_2 \leq \xi_3 < \sqrt{\xi_3}$. This means that for $\xi_2 + \xi_3 < 1$, $A < 0$ for certain, while for $\xi_2 + \xi_3 \geq 1$, $A(y_1)$ has a zero (the smaller one) within the range $0 \leq y_1 \leq \sqrt{\xi_2}$. This zero is given by

$$y_1^{(0)} = \sqrt{\xi_2\xi_3} - \sqrt{(1 - \xi_2)(1 - \xi_3)}. \quad (122)$$

For $0 \leq y_1 \leq y_1^{(0)}$, $A \geq 0$, and as $y_1^{(0)} \leq y_1 \leq \sqrt{\xi_2}$, $A < 0$. Thus, we conclude that,

- (a) For $\xi_2 + \xi_3 < 1$, there are three positive roots.
- (b) For $\xi_2 + \xi_3 \geq 1$, there are three positive roots when $\sqrt{\xi_1} > \sqrt{\xi_2\xi_3} - \sqrt{(1 - \xi_2)(1 - \xi_3)}$, and two when $\sqrt{\xi_1} \leq \sqrt{\xi_2\xi_3} - \sqrt{(1 - \xi_2)(1 - \xi_3)}$.

4. When $\xi_1, \xi_2, \xi_3 > 1$, $B < 0$. This is the opposite scenario to the one above, and there can be 2 or 1 positive roots. We adopt a similar approach as above and are able to conclude that there are two positive roots when $1 \leq \sqrt{\xi_1} \leq \sqrt{\xi_2\xi_3} - \sqrt{(\xi_2 - 1)(\xi_3 - 1)}$, and one only when $\sqrt{\xi_1} > \sqrt{\xi_2\xi_3} - \sqrt{(\xi_2 - 1)(\xi_3 - 1)}$.

To summarize, we can describe a qualitative trend of the number of positive roots of τ_g in terms of the relative strength $\epsilon_{\alpha\beta}$ of inter-species aggregations. In general, the number decrease as $\epsilon_{\alpha\beta}$'s are turned up against $f_{\alpha,\beta}$, from 3 roots to 1. Meanwhile, the smallest positive root, i.e. the physical one, shifts towards $\tau = 0$, corresponding to a speeding-up of time-to-cohesion following the increase in aggregation rate, while the other roots shift towards $\tau \rightarrow \infty$. During this shift of roots, when one of the relative interaction strength $\xi_\alpha \equiv \epsilon_{\beta\gamma}^2 / (f_\beta f_\gamma)$ is much smaller or larger than the other two, this scenario **always** corresponds to two positive roots.

In short, there is a close connection between the number of positive roots and the relative inter/intra-aggregation strengths. When all ξ_α 's are small – 3 positive roots; when one or two ξ_α 's are significantly larger than the rest – 2 positive roots; when all ξ_α 's are large – 1 positive root.

Finally, we include (Fig. 7) a numerical 3-D plot of time-to-cohesion, i.e. the smallest positive root, as a function of two of the six parameters, ξ_1, ξ_2 . As mentioned above, it does indeed decrease as $\xi_{1,2}$ increase.

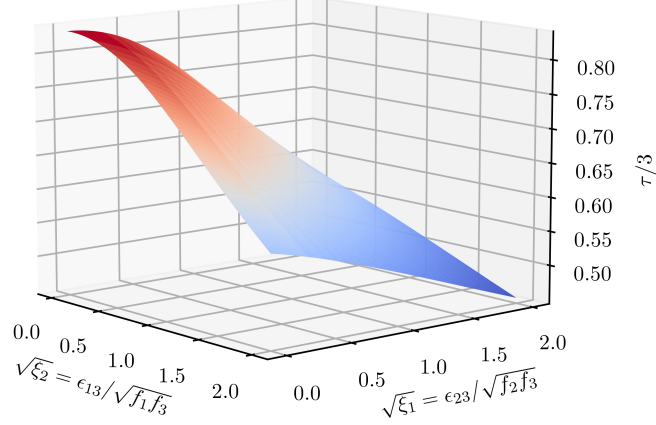


FIG. 7. Time-to-cohesion as a function of ξ_1, ξ_2 . The rest of the parameters are set at $f_1 = f_2 = 1, f_3 = 0.25, \epsilon_{12} = 0.1$.

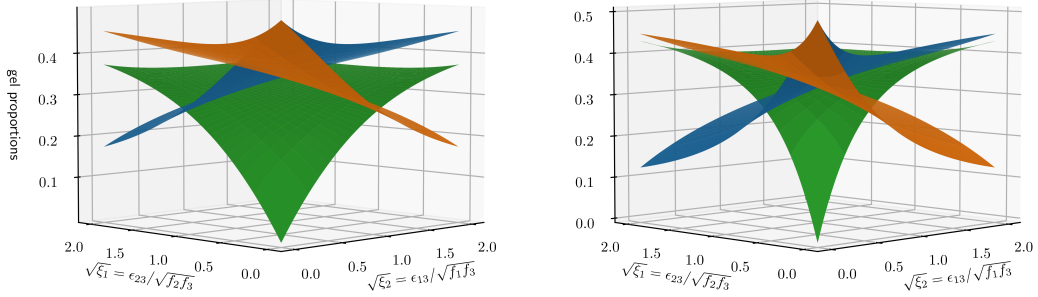


FIG. 8. The cohesive unit compositions against parameters x_1, x_2 , whilst holding $f_1 = f_2 = 0.33$ and $x_3 = 0.33$. The left graph has $f_3 = 0.2$ and the right $f_3 = 0.33$. Here we set the aggregation parameters for both species 1 (blue) and 2 (orange) to be identical, and that the coupling between species 1 and 2 is constant, hence the symmetry. The increased proportionality of species 3 (green) on the right is the result of increased f_3 and manifests the general trend mentioned above.

B. Cohesive Unit's composition

By substituting the numerically-found time-to-cohesion from the previous Section into the expressions of cohesive unit composition in Eq. (110), we are able to obtain the 3-species compositions at onset and study how they depend on the parameters. Generally speaking, larger f_α and $\epsilon_{\alpha\beta}$ should correspond to a larger proportion of species α in the cohesive unit. Nonetheless, there exist many nuances due to the high complexity as a result of no less than 6 independent parameters. They are captured in the plots of cohesive unit composition against part of the parameter space.

In the discussions below we mainly look at the behaviors of species 1 *wlog* – due to symmetry, and how changing parameters shift the behaviors. The following results follow:

1. In both plots of Fig. 8, at $\epsilon_{13} = \epsilon_{23} = 0$ species 3 is decoupled from the rest of the system, whereas species 1 and 2 dominate the cohesive unit evenly. As we turn on ϵ_{13} while keeping ϵ_{23} small, a dip in the proportion of the leading component, i.e. species 1, can be observed, even though increasing ϵ_{13} also increases the aggregation rate of species 1. In other words, turning on cross-species aggregation between two species suppresses the leading species in the cohesive unit upon cohesive unit formation, until the interaction becomes strong enough. As ϵ_{23} increases, the dip gradually disappears and species 1 in the cohesive unit becomes monotonically increasing with ϵ_{13} – this is shown in the 2-D cross-sectional diagrams in Fig. 9.

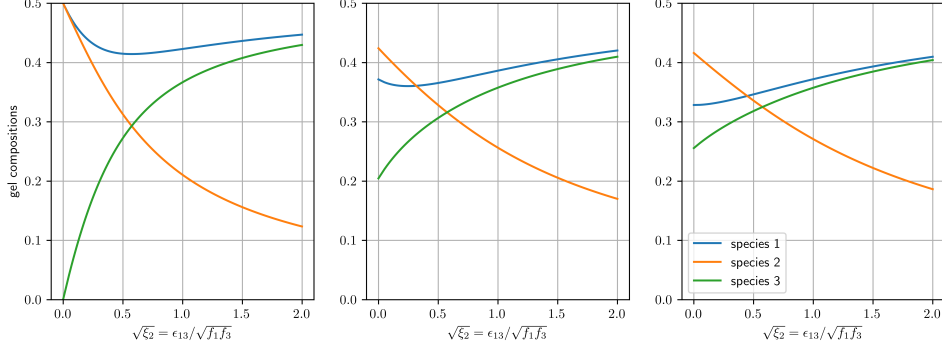


FIG. 9. Three 2-D cross-sections of cohesive unit compositions against $\sqrt{\xi_2} \propto \epsilon_{13}$, with $f_1 = f_2 = f_3 = 0.33$ and $\xi_3 = 0.33$. The ξ_1 values of the three plots are taken to be 0, 0.1, 0.2 from left to right, respectively. This shows the disappearance of the dip as ϵ_{23} increases.

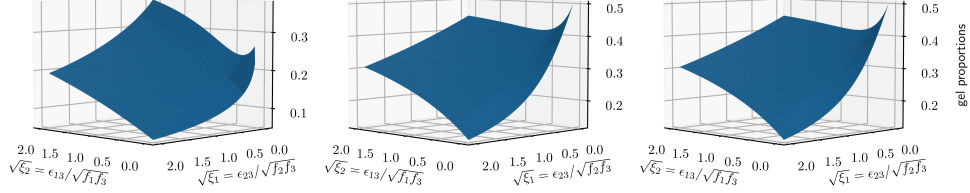


FIG. 10. Proportions of species 1 against $\sqrt{\xi_1}, \sqrt{\xi_2}$ with $f_{2,3} = \xi_3 = 0.33$, and 3 different f_1 values of 0.1, 0.33 and 0.75 from left to right. Note how the dip grows with larger f_1 .

2. Larger values of f_1 and ϵ_{12} both push this dip to grow deeper and larger along ϵ_{13} . This qualitatively means that if we have a species 1 that dominates the cohesive unit composition, introducing cross-species interaction with a new species (in this case 3) weakens this domination – and the degree of suppression is positively relevant to the level of domination. See Figs. 10 and 11.

VI. EFFECTIVE FUSION THEORY FOR MULTI-SPECIES AGGREGATION

In Section III, we have established that for a D -species aggregation system, physical cohesive unit onsets occur at $(\tau_g)_\mu = D/\lambda_\mu$ if the corresponding eigenvector $\mathbf{x}^{(\mu)}$ has no negative components. Recalling the scalar heterogeneous aggregation parameter F for 1-D systems, here we can define similar effective parameters

$$F_{\text{eff}}^{(\mu)} = \frac{\lambda_\mu}{D}. \quad (123)$$

These effective parameters may seem rather redundant, but they become useful when dimensionality D is very high and aggregation parameters $\epsilon_{\alpha\beta}$'s and f_α 's are respectively of very similar values. For such a system there exists only one physical F_{eff} , i.e. there is only one onset at $1/F_{\text{eff}}$. A good approximation of the growth-of-cohesion curve can then be written as

$$\varepsilon = e^{-F_{\text{eff}}(1-\varepsilon)\tau}, \quad (124)$$

of Eq. (39). To interpret this, we can take a coarse-grained perspective and perceive it as an effective 1-D aggregation – remember that the 1-D parameter F is in its nature a mean-field heterogeneity parameter itself. This construction

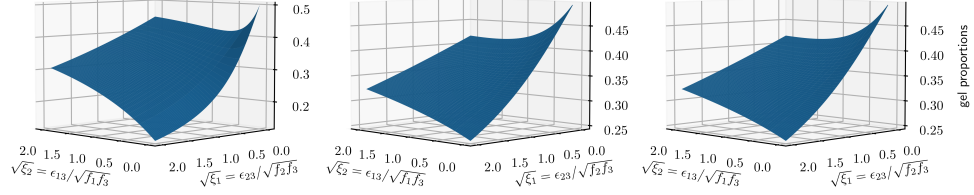


FIG. 11. Proportions of species 1 against $\sqrt{\xi_1}, \sqrt{\xi_2}$ with $f_{1,2,3} = 0.33$, and 3 different ξ_3 values of 0.33, 2.2 and 4.4 from left to right. Note how the dip grows with larger ξ_3 , i.e. larger ϵ_{12} .

shows that when D is very large, a coarse-grained model suffices and F_{eff} averages over all platforms (species) involved. This is shown in Fig. 12, which shows that the coarse-grained model (Eq. (124), plotted in orange) agrees well with the exact growth curve (Eq. (38), plotted in blue).

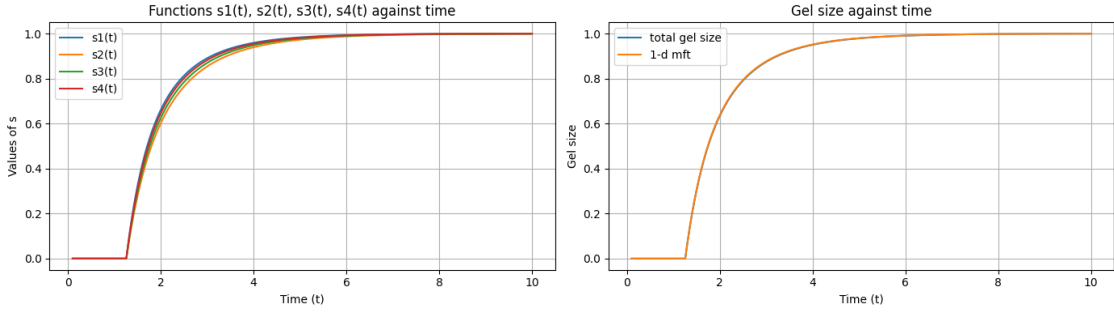


FIG. 12. For a 4-species system with similar f_α 's and $\epsilon_{\alpha\beta}$'s values, the left graph plots growth-of-cohesion curves of each species, and the right graph compares the total growth curve (sum of the left 4) against the 1-D mean-field growth curve of cohesion, where the heterogeneous parameter is taken to be the smallest of $F_{\text{eff}}^{(i)}$. The two curves highly coincide.

In order to quantitatively explore the effective fusion theory, we work under the assumption $\epsilon_{\alpha\beta} = \epsilon$ and $f_\alpha = f$ for all α, β 's. We then have

$$\omega \approx \begin{pmatrix} f & \epsilon & \cdots & \epsilon \\ \epsilon & f & \cdots & \epsilon \\ \vdots & \vdots & \ddots & \vdots \\ \epsilon & \epsilon & \cdots & f \end{pmatrix}. \quad (125)$$

By inspection, we can easily find that the normalized vector

$$\mathbf{v} = \frac{1}{\sqrt{D}} \begin{pmatrix} 1 \\ 1 \\ \vdots \\ 1 \end{pmatrix} \quad (126)$$

is an eigenvector of ω with its corresponding eigenvalue being

$$\lambda = f + (D - 1)\epsilon. \quad (127)$$

Perron-Frobenius theorem ensures that \mathbf{v} is the only physical eigendirection for cohesive unit formation, and thus there is only one onset, at time $\tau_g = D/[f + (D - 1)\epsilon]$, and correspondingly,

$$F_{\text{eff}} = \frac{f + (D - 1)\epsilon}{D}. \quad (128)$$

This gives directly the result stated in the main paper (Eq. (4)). When $D \rightarrow \infty$, $F_{\text{eff}} \approx \epsilon$, we can see that $F_{\text{eff}} \approx \epsilon$ – in other words, multi-species aggregation recovers to a cross-platform interaction process. Moreover, from Eq. (38) we can further deduce that in this scenario, the growth-of-cohesion curves for all D species satisfy the following equation:

$$\varepsilon_\alpha = e^{-[f(1-\varepsilon_\alpha)+\epsilon \sum_{\beta \neq \alpha} (1-\varepsilon_\beta)]\tau/D}, \quad \alpha = 1, \dots, D. \quad (129)$$

These D equations are identical, so all of the D species must reach cohesion simultaneously (as we concluded earlier) and their growth curves must also be identical. Hence, the combined growth curves for the whole system must retain the simple shape of a 1-D one.

VII. SUMMARY OF OUR NOTATION AND POTENTIAL ADDITIONS TO THE THEORY

A. Our notation in the main paper

First we summarize the suffix notations we have used throughout the paper and SM for clarification purpose.

1. The subsystems i.e. coupled species that are decoupled from the rest of the fusion system are labelled as s . Matrix F can be written as block diagonal form of d irreducible submatrices F_s .
2. Species are labelled with Greek letters. In particular, physical species (species $1, 2, \dots, D$) are labelled as α, β , etc. e.g. the components of the heterogeneity matrix $F_{\alpha\beta}$ and the vector component of size profile k_α . The mixed composition of a cohesive unit, are labelled by μ, ν , such as in the eigenvectors $\mathbf{x}^{(\mu)}$ and eigenvalues λ_μ of matrix F . They all take values from 1 to D .
3. Cluster sizes are labelled with i, j, k etc. — for D -dimensional systems they are vectors $\mathbf{i}, \mathbf{j}, \mathbf{k}$ etc.. Components i_α, j_β , etc. represent numbers of entities with species type α, β etc. within cluster i, j etc..
4. Entities are labelled with p, q , etc., so vector $\vec{y}_{p;\alpha}$ represents the trait of an α species entity labelled as p . These two parameters together label the entities.

B. Potential additions to the theory

This theory is easily extended to include other online mechanisms. Here we summarize some of them:

- (1) Introducing an exponential decay $e^{-\mathbf{a} \cdot (\mathbf{k}_1 + \mathbf{k}_2)}$ to the product kernel in Eq. (15) adds a non-local term $\varepsilon(\mathbf{x} + \mathbf{a}, t)$ to Eq. (32).
- (2) Adding a multi-community ($\chi > 2$) product kernel $\prod_{m=1}^\chi k_{\alpha_m}$, $1 \leq \alpha_m \leq D$ to Eq. (21) to mimic a coordinated campaign [48], together with a rank- χ heterogeneity mean-field tensor $F_{\alpha_1 \dots \alpha_\chi}$, adds $F_{\alpha_1 \dots \alpha_\chi} \varepsilon_{\alpha_1}(\mathbf{x}, t) \dots \varepsilon_{\alpha_\chi}(\mathbf{x}, t)$ to Eq. (28). For the Burgers-like equation Eq. (32), this corresponds to $F_{\alpha_1 \dots \alpha_\chi} \varepsilon_{\alpha_1} \dots \varepsilon_{\alpha_{\chi-1}} \partial_{\alpha_\chi} \varepsilon_\alpha$.
- (3) Any reversed process of aggregation that reduces cohesion can be mimicked by fragmentation terms akin to that in Ref. [36].
- (4) Shifts in background population mood and influxes of new particles in response to external events, can be mimicked by changes in $F(t)$ and $N_\alpha(t)$ [32].
- (5) Entities' individual loss of 'interest' can be mimicked by adding monomer fragmentation terms.
- (6) The presence of influencers can be mimicked by making the aggregation favor their particular $\vec{y}_{p;\alpha}(t)$ values.
- (7) The influence of external actors can be mimicked by biasing subsets of $\vec{y}_{p;\alpha}(t)$ over time, as can the influence of so-called digital inoculation schemes.
- (8) Much research has also focused on the spreading of harmful content including mis(dis)information: this could be mimicked by adding a viral process (e.g. SIR [21]) into the generative equation. However, until the correct viral

process is established for online material, it makes more sense to focus on the total number of links available since this is ultimately what amplifies the traffic and encourages further growth of anti-X communities: adding $|\mathbf{k}|^2 \nu_{\mathbf{k}}(t)$ to Eq. (21) (which for large $|\mathbf{k}|$ measures links within each and every species for all aggregates of size \mathbf{k}) adds a diffusive term $\nabla^2 \varepsilon(\mathbf{x}, t)$ to Eq. (32).